Isoindolo[2,1-*a*]quinoxaline Derivatives, Novel Potent Antitumor Agents with Dual Inhibition of Tubulin Polymerization and Topoisomerase I

Patrizia Diana,*[,†] Annamaria Martorana,[†] Paola Barraja,[†] Alessandra Montalbano,[†] Gaetano Dattolo,[†] Girolamo Cirrincione,[†] Francesco Dall'Acqua,[‡] Alessia Salvador,[‡] Daniela Vedaldi,[‡] Giuseppe Basso,[§] and Giampietro Viola[‡]

Dipartimento Farmacochimico Tossicologico e Biologico, Università degli Studi di Palermo, Via Archirafi 32, 90123 Palermo, Italy, Dipartimento di Scienze Farmaceutiche, Università degli Studi di Padova, Via Marzolo 5, 35131 Padova, Italy, and Dipartimento di Pediatria, Università degli Studi di Padova, Via Giustiniani 3, 35131 Padova, Italy

Received July 10, 2007

Isoindoloquinoxalines **4** and **5** were obtained by refluxing 2-(2′-aminoaryl)-1-cyanoisoindoles **3a**−**e** in acetic or formic acid. All derivatives were screened by the National Cancer Institute (Bethesda, MD) for the in vitro one dose primary anticancer assay against a 3-cell line panel. Compounds **4a**−**e**, screened against a panel of about 60 human tumor cell lines, showed remarkable antineoplastic activity; they had GI_{50} values in the low micromolar or submicromolar range and reached, in the case of **4c**, nanomolar concentrations on 88% of the 59 tested cell lines. Flow cytometric analysis of cell cycle after treatment with **4c** demonstrated an arrest of the cell cycle in G2/M phase. This effect was accompanied with apoptosis of the cells, mitochondrial depolarization, generation of reactive oxygen species, and activation of caspase-3 and caspase-9. Moreover, **4c** induced a clear increase in the mitotic index, inhibited microtubule assembly in vitro, and interestingly also acted as a topoisomerase I inhibitor.

Introduction

DNA represents one of the most important targets for several chemotherapeutic drugs. Polycyclic nitrogen heterocycles with planar structure can be good pharmacophores for classes of antitumor drugs because they can intercalate between the base pairs of double-stranded DNA. Well-known cancer chemotherapeutic agents, such as anthracyclines, camptothecin, and amsacrine (Chart 1), characterized by planar polycyclic systems, are able to interfere with DNA-processing enzymes (topoisomerases I and II) by forming a ternary complex involving the drug, the DNA, and the enzyme.[1]

Quinoxalines and the structurally related quinoxalinones represent an important class of compounds that are found in a variety of biologically and medicinally useful agents. A large number of synthetic quinoxalines showed antineoplastic activity.[2] For instance, substituted (phenoxymethyl)quinoxalinones demonstrated excellent antagonism of P-glycoprotein and multidrug resistant protein (MRP1)[a] in drug-resistant cell lines.[3] A quinoxaline ring condensed with a pyridine moiety led to benzo[*f*]pyrido[4,3-*b*] and pyrido[3,4-*b*]quinoxalines derivatives which showed topoisomerases inhibition.[4] Incorporation of an indole ring gave 5-substituted 2-bromoindolo[3,2-*b*]quinoxalines that showed a broad spectrum of antitumor activity with two biochemical mechanism-based screens (cdc2 kinase and cdc25 phosphatase) with IC_{50} of 70 and 25 μM, respectively.[5]

Continuing our research on polycyclic heterocycles containing the pyrrole or indole moieties with antineoplastic activity,[6] and in our attempts to search for novel antitumor compounds, we extended our interest to the isoindole system and planned to synthesize isoindolo[2,1-*a*]quinoxaline derivatives in order to evaluate their antiproliferative activity and their targets at cellular and molecular levels.

Chemistry

Our approach to the isoindoloquinoxaline nucleus involved the annelation of a quinoxaline ring on the isoindole moiety by using suitably substituted 2-(2′-aminoaryl)-1-cyano-isoindoles of type **3** as key intermediates. This synthetic route allowed easy functionalization of the quinoxaline moiety, low cost and easily available starting material, and high yields. Only two isoindoloquinoxaline derivatives of type **5** were incidentally obtained during attempts to synthesize the benzoimidazo[2,1-*a*]isoquinoline system. As a matter of fact, reaction of 2-alkynylarylaldehydes with 1,2-phenylendiamine led to an inseparable mixture of the desired system and the unexpected isoindolo[2,1-*a*]quinoxaline in low yields. The components of the mixture, rather sensitive, could be characterized only as HBF_4 salts.[7]

The isolation of derivative **3** was possible by a Strecker-type synthesis between substituted 1,2-phenylendiamine **1** and phthalaldehyde **2** in water and in the presence of potassium cyanide and sodium hydrogensulfite.[8] In the case of 3-methyl-1,2-phenylendiamine **1b**, along with **3b** was also isolated the isomer 1-cyano-2-(2′-amino-6′-methylphenyl)isoindole. On the other hand, in the case of 4-methoxy-1,2-phenylendiamine **1c**, only derivative **3c** was isolated because of the enhanced reactivity of the amino group placed in the *para* position with respect to the methoxy substituent (Scheme 1).

Isoindole quinoxalines **4a**−**e** were prepared by reaction of the isoindole intermediates **3a**−**e**. Refluxing these latter in acetic acid brought about the reaction of the amino group with the carbonitrile group, leading to the quinoxaline ring system. In

* Corresponding author. Phone: +39-091-6161606. Fax: +39-091-6169999. E-mail: diana@unipa.it.

† Dipartimento Farmacochimico Tossicologico e Biologico, Università degli Studi di Palermo.

‡ Dipartimento di Scienze Farmaceutiche, Università degli Studi di Padova.

§ Dipartimento di Pediatria, Università degli Studi di Padova.

[a] MRP1, multidrug resistant protein; st-DNA, salmon testes DNA; ICD, induced circular dichroism; PI, propidium iodide; LD, linear dichroism; LD_r, reduced LD; PS, phosphatidylserine; ROS, reactive oxygen species; HE, hydrohethidine; NAO, 10-nonyl acridine orange; FITC, fluorescein isothiocyanate; TRITC, tetramethyl rhodamine isothiocyanate; JC-1, 5,5′,6,6′-tetrachloro-1,1′,3,3′-tetraethylbenzimidazolcarbocyanine; NCI, National Cancer Institute; TGI, total growth inhibition; MG_MID, mean graph midpoint; P-gp, P-glycoprotein; CD, circular dichroism; HBSS, Hank's balanced salt solution; BSA, bovine serum albumin.

10.1021/jm070834t CCC: $40.75
Published on Web 03/27/2008

Scheme 1.

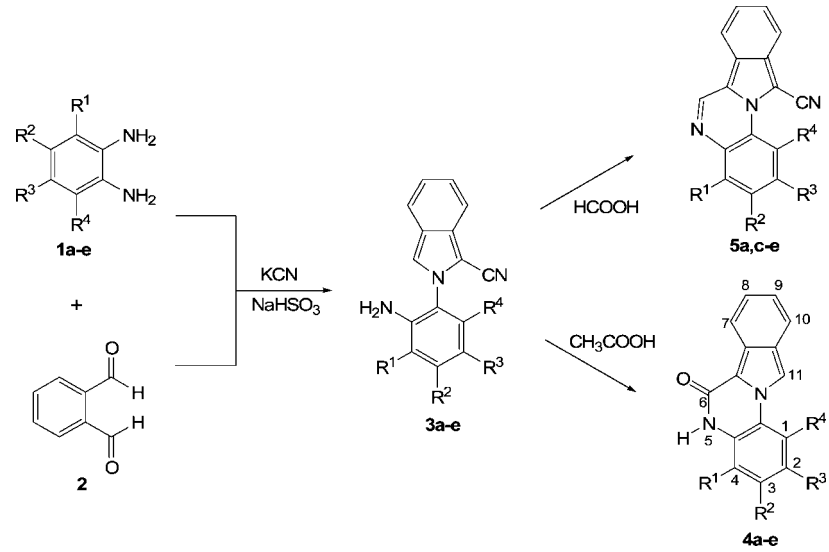

Chart 1

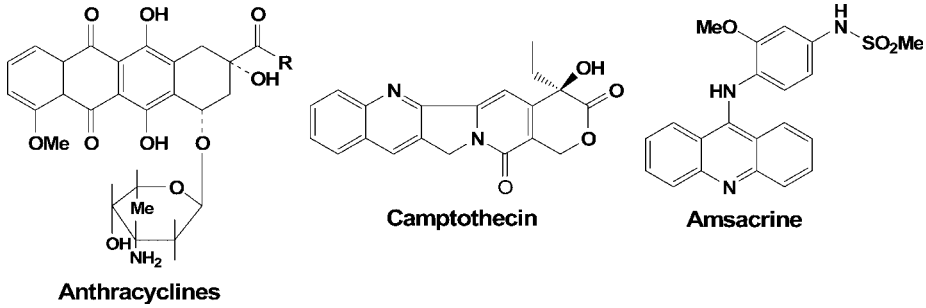

situ hydrolysis of the formed imine moiety gave isoindoloquinoxalinones **4a**−**e** in excellent yields. Derivatives of the same ring system of type **5** were obtained, in excellent yields, by reaction of intermediates **3** with refluxing formic acid (Scheme 1). However, the reaction of **3b** with formic acid originated a very complex mixture from which it was impossible to isolate **5b**. The structure of all synthesized compounds was confirmed by their analytical and spectral data (IR, ^{1}H NMR, and ^{13}C NMR).

Biological Results and Discussion

Antitumor Activity (in Vitro Growth Inhibition and Cytotoxicity). The isoindoloquinoxaline derivatives **4a**−**e** and **5a,c**−**e** were evaluated by the National Cancer Institute (NCI, Bethesda, MD) in the 3-cell line (MCF7-breast, NCI-H460-nonsmall cell lung, and SF-268-CNS), one dose primary anticancer assay (10^{-4} M) (Table 1). A compound was considered as active when it reduced the growth of any of the cell lines to 32% or less (negative numbers indicate cell kill). The compounds which satisfied the criteria set by the NCI for activity in this assay were scheduled automatically for evaluation against the full panel of tumor cell lines.[9] All isoindoloquinoxaline derivatives of type **4** were selected for evaluation against the full NCI panel of approximately 60 human cancer cell lines grouped in disease subpanels including leukemia, nonsmall-cell lung, colon, central nervous system, melanoma, ovarian, renal, prostate, and breast tumors cell lines. The following parameters were determined for every cell line: GI_{50} (concentration inhibiting 50% net cell growth), TGI (total growth inhibition), and LC_{50} (concentration leading to 50% net cell death). The average values of mean graph midpoint (MG_MID) were calculated for each of these parameters.[10] Isoindoloquinoxaline derivatives **5**, at the dose of 10^{-4} M, showed to be inactive against the three cell lines mentioned above, likely because of the lack of lactam moiety in the quinazoline nucleus.

Table 1. One Dose Primary Anticancer Assay for Isoindoloquinoxalines **4a–e** and **5a,c–e**

compd	nonsmall cell-lung NCI-H460	breast MCF7	CNS SF-268	compd selected for 60 cell
4b	0	6	9	Y
4b	2	27	55	Y
4c	0	0	1	Y
4d	0	0	0	Y
4e	0	10	13	Y
5a	91	107	94	N
5c	97	115	96	N
5d	78	97	83	N
5e	104	108	104	N

An evaluation of the data reported in the Table 2 points out that compounds **4a**−**e** exhibited antineoplastic activity against all the human cell lines. The most active compound was the 3-methoxy derivative **4c** (MG_MID = 7.32), followed by 4-methyl **4b**, unsubstituted **4a**, and 2,3-dimethyl **4d** derivatives, which showed similar MG_MID values (5.28, 5.17, and 4.99, respectively). The 2,3-dichloro derivative **4e** (MG_MID = 4.74) was the least active. From the available data, it seems that substituents that enriched the π-electron density of the benzene moiety of the quinoxaline system improved the antineoplastic

Table 2. Overview of the Results of the in Vitro Antitumor Screening for Compounds **4a–e**[a]: Number of Cell Lines Giving Positive pGI_{50}, pTGI, and pLC_{50}

		pGI_{50}[b]			pTGI[c]			pLC_{50}[d]		
cpd	no.[e]	N[f]	range	MG_MID[g]	N[f]	range	MG_MID[g]	N[f]	range	MG_MID[g]
4a	57	57	6.28–4.60	5.17	49	5.20–4.05	4.5	30	4.50–4.07	4.11
4b	57	57	>8.00–4.51	5.28	48	5.38–4.03	4.53	22	4.90–4.02	4.12
4c	59	59	8.39–5.29	7.32	59	7.68–4.51	5.87	44	6.30–4.06	5.20
4d	57	57	5.80–4.60	4.99	55	5.51–4.22	4.57	50	5.21–4.01	4.21
4e	56	56	6.09–4.48	4.74	53	4.73–4.12	4.42	43	4.27–4.03	4.16

[a] Data obtained from the NCI's in vitro disease-oriented human tumor cells screen. [b] pGI_{50} is the $-\log$ of the molar concentration that inhibits 50% net cell growth. [c] pTGI is the $-\log$ of the molar concentration giving total growth inhibition. [d] pLC_{50} is the $-\log$ of the molar concentration leading to 50% net cell death. [e] Number of the cell lines investigated. [f] Number of cell lines giving positive GI_{50}, TGI, and LC_{50}. [g] MG_MID (mean graph midpoint) is the arithmetical mean value for all tested cancer cell lines. If the indicated effect was not attainable within the used concentration interval, the highest tested concentration was used for the calculation.

activity. The fact that the 2,3-disubstituted derivatives were the least active indicates that substituents in position 2 were not tolerated.

The isoindoloquinoxalines showed inhibitory effects in the growth of all cancer cell lines from micromolar to nanomolar concentration (Table 3). Derivatives **4**, with the exception of **4e**, were particularly effective against the leukemia subpanel. In fact, the calculated MG_MID values for the leukemia subpanel were always higher than the overall cell lines MG_MID values (ΔMG_MID = 0.24−0.51).

Table 3 shows that compound **4c** was selective toward 88% of the tested cell lines and had GI_{50} values at the 10^{-8} M level. The most sensitive cell lines were HL-60 (TB) (pGI_{50} 7.94), SR (pGI_{50} 8.00), and K562 (pGI_{50} 8.05), belonging to the leukemia subpanel; MALME-3 M (pGI_{50} 8.00) and M14 (pGI_{50} 8.00) of the melanoma subpanel; and MDA-MB-435 (pGI_{50} 8.39), belonging to the breast cancer subpanel.

Compound **4b**, bearing a methyl group in position 4, showed excellent response in the breast cancer subpanel, besides exhibiting selectivity with respect to the leukemia subpanel. The most sensitive cell lines were MCF7 (pGI_{50} > 8.00), MDA-MB-231/ATCC (pGI_{50} 5.62), and MDA-MB-435 (pGI_{50} 5.50). Derivative **4a** was selectively active with respect to breast cancer and especially active against HS 578T (pGI_{50} 6.28) and MDA-MB-231/ATCC (pGI_{50} 6.02).

The dichloro derivative **4e** had a low pGI_{50} mean value (4.74) but showed a good selectivity with respect to the HCC-2998 cell line (pGI_{50} 6.09), belonging to the colon cancer subpanel.

In Table 4, the pTGI and pLC_{50} values of compounds **4a**−**e** are reported.

At TGI level, the most interesting compound was **4c**, both in terms of pTGI values (MG_MID = 5.87) and in terms of activity against the total number of cell lines (59), followed by **4d**, **4b**, **4a**, and **4e** (MG_MID in the range 4.42−4.57 and number of sensitive cell lines in the range 48−55). Compound **4c** showed good selectivity with respect to the MDA-MB-435 (pTGI 7.68) and NCI/ADR-RES (pTGI 7.24) cell lines of the breast cancer subpanel, the HCC-2998 (pTGI 7.31) cell lines of the colon subpanel, the HL-60(TB) (pTGI 7.22) of the leukemia subpanel, OVCAR-3 (pTGI 7.19) of the ovarian subpanel, and SF-539 (pTGI 7.15) and SNB-75 (pTGI 7.08) of the CNS subpanel.

At LC_{50} level, the best response was observed in the case of the HCC-2998 (pLC_{50} 6.30) colon cancer cell lines obtained by **4c**.

Effect of Isoindolo[2,1-*a*]quinoxalines on Multidrug Resistant Cell Lines. Although many anticancer drugs in clinical use are effective in the treatment of different kinds of tumors, their potential is limited by the development of drug resistance. Resistance can be intrinsic or acquired, but in either case, tumors become refractory to a variety of structurally different drugs.

Thus, the antiproliferative effects of isoindolo[2,1-*a*]quinoxalines **4a**−**e** were evaluated in three human cancer cell lines expressing high level of 170-kDa P-glycoprotein (P-gp) drug efflux and MRP. As shown in Table 5, the examined compounds are equally potent toward (i) parental cells, (ii) cells resistant to vinblastine and doxorubicine, and (iii) cell sublines resistant to different drugs.

Cell Cycle Analysis. In order to clarify the mechanism(s) of action of the isoindoloquinoxalines, the effects of different concentrations of the most active compound **4c** on cell cycle progression of Jurkat cells (pGI_{50} = 8.39) after 24 h of drug exposure were studied. The cell cycle histograms, based on flow cytometric analyses of **4c** at different concentrations, are illustrated in Figure 1. It can be noted that treatment of Jurkat cells with **4c** at low concentrations led to profound changes of the cell cycle profile. Untreated cells showed a classical pattern of proliferating cells proportionally distributed in G1 (48%), S (37%), and G2/M (15%) phases. On the contrary, a clear and rapid G2/M arrest pattern (lower panel) was observed with a concomitant decrease of the G1 phase. It was also interesting to note the appearance of a hypodiploid peak (sub-G1), indicative of apoptosis, which reached the value of 35% at the concentration of 62.5 nM.

Mitotic Index. Because **4c** caused a massive cell accumulation in the G2/M phase, the appearance of mitotic cells was quantitatively analyzed. The cells were recognized by optical microscopy by the presence of dispersed chromosomes in the cytoplasm and by the disappearance of the nuclear membrane. It was found that the percentage of mitotic cells (the mitotic index) increased in a concentration-dependent manner upon treatment (Figure 2), well in accordance with the cell cycle analysis data. The concentration needed to arrest 50% of Jurkat cells at mitosis was about 0.5 μM for compound **4c** and was similar to that of colchicine used as reference drug.

Immunofluorescence Microscopy. As further proof of these new derivatives interfering with the microtubule network, compound **4c** was checked by immunofluorescence microscopy. For these experiments, we used a nonsmall cell lung carcinoma (A-549) cell line. As shown in Figure 3 (panel A), the microtubule network in control cells exhibited normal organization and arrangement. On the contrary, compound **4c**, at different concentrations and after 24 h of incubation, (panels C 5 μM and D 2.5 μM) completely disrupted the tubulin network. Cells showed an evident characteristic rounded-up morphology caused by disaggregation of microtubules in both interphase and mitotic phases after 24 h of treatment. These effects resembled those of vinblastine chosen as reference compound (panel B).

Effect of Isoindolo[2,1-*a*]quinoxaline 4a–e on Microtubule Polymerization in Vitro. As the immunofluorescence studies suggested that **4c** impaired the formation or the stability

Table 3. Inhibition of in Vitro Cancer Cell Lines by Isoindolo[2,1-*a*]quinoxalines **4a–e**[a]

cell line	pGI$_{50}$[b]				
	4a	**4b**	**4c**	**4d**	**4e**
Leukemia					
CCRF-CEM	5.23	5.92	7.52	5.00	4.66
HL-60 (TB)	ND[c]	ND	7.94	ND	ND
RPMI-8226	5.43	5.70	7.44	5.17	4.65
MOLT-4	5.44	5.74	7.11	5.25	4.73
SR	5.54	5.81	8.00	5.59	4.76
K-562	ND	ND	8.05	ND	ND
Nonsmall Cell Lung Cancer					
A549/ATCC	5.23	5.30	7.17	4.83	4.72
EKVX	5.32	5.25	7.04	4.87	4.66
HOP-62	5.36	5.45	7.51	5.57	ND
HOP-92	5.40	5.40	6.00	4.81	4.74
NCI-H226	5.54	5.49	7.34	4.82	4.73
NCI-H23	4.95	4.76	7.37	4.83	4.76
NCI-H322M	4.62	4.87	7.08	4.78	4.87
NCI-H460	5.11	5.72	7.46	5.35	4.73
NCI-H522	4.86	5.19	7.22	4.84	4.99
Colon Cancer					
COLO-205	5.34	5.13	7.39	4.82	4.53
HCC-2998	5.23	5.34	7.74	5.39	6.09
HCT-116	5.67	5.57	7.40	5.80	4.68
HCT-15	5.48	5.28	7.58	5.21	4.78
HT29	5.36	5.66	7.47	5.22	4.54
KM12	4.72	5.47	7.48	5.15	4.76
SW-620	5.43	5.24	7.58	5.42	4.80
CNS Cancer					
SF-268	4.67	5.52	7.13	4.81	4.62
SF-295	4.75	5.58	7.57	4.91	4.79
SF-539	5.29	5.41	7.64	4.95	4.72
SNB-19	5.05	4.81	7.41	4.79	4.66
SNB-75	4.87	4.51	7.56	4.81	4.67
U251	5.49	5.18	7.36	5.39	4.79
Melanoma					
LOX IMVI	5.52	5.21	7.15	5.69	4.76
MALME-3M	4.60	5.08	8.00	4.65	4.77
M14	5.19	4.90	8.00	4.87	4.64
SK-MEL-2	4.69	4.84	6.80	4.74	4.60
SK-MEL-28	4.65	5.16	7.28	4.83	4.48
SK-MEL-5	5.72	4.93	7.55	4.87	4.70
UACC-257	4.82	4.78	5.29	4.69	4.69
UACC-62	5.49	5.16	7.13	4.78	4.78
Ovarian Cancer					
IGROV1	4.99	5.43	7.13	4.91	4.76
OVCAR-3	4.73	5.32	7.65	4.86	4.73
OVCAR-4	5.14	5.17	7.04	4.87	4.69
OVCAR-5	4.98	4.75	7.00	4.86	4.77
OVCAR-8	5.28	5.45	7.24	5.15	4.73
SK-OV-3	4.91	4.56	7.41	4.74	4.74
Renal Cancer					
786–0	5.37	5.23	7.38	4.97	4.60
A498	4.95	4.79	7.65	4.67	4.80
ACHN	5.74	5.39	6.90	4.99	4.81
CAKI-1	4.75	5.66	7.45	5.27	4.69
RXF 393	5.20	5.04	7.69	4.92	4.76
SN12C	5.78	5.74	7.24	5.22	4.80
TK-10	4.69	4.57	6.29	4.70	4.78
UO-31	4.90	5.25	7.10	4.84	4.75
Prostate Cancer					
PC-3	5.24	5.41	7.43	4.92	4.76
DU-145	5.12	5.28	7.58	4.86	4.75
Breast Cancer					
MCF7	4.98	>8.00	7.55	4.93	4.67
NCI/ADR-RES	5.19	4.92	7.67	4.87	4.75
MDA-MB-231/ATCC	6.02	5.62	7.25	5.08	4.76
HS 578T	6.28	4.66	7.29	4.60	4.70
MDA-MB-435	4.79	5.50	8.39	5.22	4.77
BT-549	4.72	4.92	7.26	4.71	4.58
T-47D	5.13	4.94	7.32	4.81	4.51
MG_MID[d]	5.17	5.28	7.32	4.99	4.74

[a] Data obtained from NCI's in vitro disease-oriented tumor cells screen. [b] pGI$_{50}$ is the −log of the molar concentration causing 50% growth inhibition of tumor cells. [c] ND: not determined. [d] MG_MID (mean graph midpoint) is the arithmetical mean value for all tested cancer cell lines. If the indicated effect was not attainable within the used concentration interval, the highest tested concentration was used for the calculation.

of microtubules in the cells and microtubules are the major apparatus responsible for mitotic division, the effects of isoindolo[2,1-*a*]quinoxaline **4a**−**e** on the polymerization of microtubule protein isolated from porcine brain were examined. The assay utilized a fluorescent compound which binds to tubulin and microtubules. Polymerization was followed by fluorescent enhancement because of incorporation of a fluorescent reporter into the microtubules as polymerization occurred.[11] Figure 4 shows that in the control sample (tubulin alone without addition of any test agent), the fluorescence increased over time. On the contrary, the tested compounds **4a**−**e** clearly induced a concentration-dependent inhibition of tubulin polymerization. In particular, a complete inhibition of microtubule assembly was observed for **4c** at a concentration of 5 μM. Colchicine, the reference drug, completely inhibited the tubulin polymerization at a concentration of 3 μM, whereas at the same concentration, Taxol significantly promoted tubulin polymerization (data not shown). The other derivatives presented a similar behavior, although a complete inhibition of the tubulin polymerization was observed at concentrations higher than 10 μM. In further experiments, the effects of **4c** on preassembled microtubules were investigated. None of the tested compounds were able to induce microtubule depolymerization (data not shown), indicating that the action of these compounds was strictly related to the interference with microtubule assembly.

DNA Binding Studies. As isoindolo[2,1-*a*]quinoxaline **4a**−**e** exhibit a planar structure, the interaction of compound **4c,** as representative, with DNA was evaluated with a series of spectrophotometric studies. The binding of **4c** to DNA in buffered aqueous solution was monitored by absorption and fluorescence spectroscopy (Figure 5). The absorption of the compound was recorded both in the absence and in the presence of salmon testes DNA (st-DNA). The maximum absorption of compound **4c** exhibited a weak bathochromic shift of about 2 nm with respect to the free drug in the presence of nucleic acid (Figure 5A); **4c** also showed a hypochromism of the signal intensity, suggesting the association of the drug with DNA. Most notably, isosbestic points appeared in the titration, indicating that one type of drug−DNA complex was almost exclusively formed. The spectrophotometric titration data for **4c** bound to the DNA were used to estimate the binding constant as well as binding-site size according to McGhee and von Hippel.[12] The corresponding binding isotherm, represented as a Scatchard plot,[13] is presented in the inset of Figure 5A). The binding constants K revealed a high binding affinity of **4c** ($K = 2.7 \times 10^5$ M^{-1}), and the binding-site size n was 3.6 (in bases), in accordance with the intercalative binding mode used in the neighbor-exclusion model.[12] Spectrofluorometric titrations of st-DNA to compound **4c** were also performed (Figure 5B). The emission intensity of the free drug was quenched upon addition of st-DNA without any shift of the emission maximum.

The Stern−Volmer plot derived from the fluorimetric titration of st-DNA exhibited linear behavior of the titration curve up to a concentration of 40 μM (Figure 5B). From these data, quenching efficiency was estimated by the Stern−Volmer constant K_{SV} (**4c**: $K_{SV} = 31765$ M^{-1}).

To further study the interaction of **4c** with DNA, circular dichroism (CD) spectra of DNA in the presence of increasing concentration of **4c** were recorded. The CD spectra of DNA revealed a significant perturbation of the DNA signal because the positive CD band of the DNA at 275 nm increased upon successive addition of **4c** (Figure 6, upper panel). Also, significant positive induced CD (ICD) signals were observed in the chromophore absorption region of **4c** (300−400 nm),

Table 4. Inhibition of in Vitro Cancer Cell Lines by Isoindolo[2,1-*a*]quinoxalines **4a–e**[a]

	pTGI[b]					pLC$_{50}$[c]				
cell line	**4a**	**4b**	**4c**	**4d**	**4e**	**4a**	**4b**	**4c**	**4d**	**4e**
					Leukemia					
CCRF-CEM	4.22	4.90	5.84	4.51	4.31	<4.00	4.13	<4.00	4.01	<4.00
RPMI-8226	4.65	5.15	5.85	4.53	4.31	<4.00	4.22	5.16	<4.00	<4.00
MOLT-4	5.06	5.25	5.67	4.71	4.43	<4.00	4.68	4.12	4.15	4.14
SR	5.11	5.38	5.69	5.24	4.41	<4.00	4.90	4.12	4.31	4.06
HL-60 (TB)	ND[d]	ND	7.22	ND	ND	ND	ND	5.45	ND	ND
K-562	ND	ND	5.99	ND	ND	ND	ND	5.29	ND	ND
					Nonsmall Cell Lung Cancer					
A549/ATCC	4.49	<4.00	5.78	4.42	4.46	<4.00	<4.00	5.22	4.02	4.20
EKVX	4.16	4.35	4.53	4.50	4.36	<4.00	<4.00	<4.00	4.12	4.06
HOP-62	4.75	4.82	5.91	5.09	ND	4.28	4.29	5.41	4.54	ND
HOP-92	4.73	4.49	4.80	4.52	4.46	4.29	<4.00	4.40	4.23	4.18
NCI-H226	4.86	4.56	6.28	4.44	4.45	4.26	<4.00	<4.00	4.05	4.16
NCI-H23	4.44	4.41	5.47	4.49	4.51	<4.00	4.06	<4.00	4.16	4.25
NCI-H322M	4.33	4.34	5.59	4.52	4.57	4.05	<4.00	5.11	4.26	4.26
NCI-H460	<4.00	5.00	5.95	4.69	4.48	<4.00	4.50	5.29	4.20	4.24
NCI-H522	4.49	4.19	5.64	4.51	4.51	4.12	<4.00	5.00	4.18	4.03
					Colon Cancer					
COLO-205	<4.00	4.46	5.94	<4.00	4.40	<4.00	<4.00	5.24	<4.00	<4.00
HCC-2998	4.68	4.79	7.31	4.78	4.73	4.24	4.39	6.30	4.30	4.36
HCT-116	4.91	4.93	5.88	5.51	4.45	4.31	4.47	5.35	5.21	4.23
HCT-15	4.73	4.50	5.94	4.66	4.52	4.03	<4.00	5.34	4.21	4.26
HT29	<4.00	4.88	5.83	<4.00	<4.00	<4.00	4.44	<4.00	<4.00	<4.00
KM12	4.40	4.64	5.82	4.67	4.51	4.08	<4.00	5.22	4.28	4.25
SW-620	<4.00	4.75	5.85	4.48	4.53	<4.00	4.37	5.38	<4.00	4.27
					CNS Cancer					
SF-268	4.06	5.07	5.53	4.49	4.37	<4.00	4.12	4.06	4.16	4.12
SF-295	4.45	4.60	5.98	4.55	4.52	4.15	<4.00	5.38	4.18	4.26
SF-539	4.65	4.80	7.15	4.57	4.40	4.12	4.39	5.56	4.19	4.09
SNB-19	<4.00	4.32	5.39	4.44	4.25	<4.00	<4.00	<4.00	4.08	<4.00
SNB-75	4.13	<4.00	7.08	4.52	4.27	<4.00	<4.00	<4.00	4.23	<4.00
U251	4.87	4.71	5.82	4.85	4.52	4.15	4.34	5.30	4.32	4.26
					Melanoma					
LOX IMVI	4.92	4.74	5.75	5.40	4.51	4.07	4.37	5.35	5.10	4.25
MALME-3M	4.33	4.61	5.47	4.43	4.49	4.07	4.17	5.07	4.20	4.20
M14	4.64	4.51	4.89	4.57	4.40	4.19	4.11	5.44	4.28	4.16
SK-MEL-2	4.41	<4.00	5.60	4.46	4.27	4.14	<4.00	5.11	4.18	<4.00
SK-MEL-28	<4.00	<4.00	5.60	4.45	<4.00	<4.00	<4.00	5.18	4.08	<4.00
SK-MEL-5	4.83	4.62	5.93	4.53	4.38	4.22	4.31	5.46	4.19	4.06
UACC-257	4.48	4.03	4.51	4.45	4.31	4.14	<4.00	4.13	4.20	<4.00
UACC-62	4.80	4.55	5.72	4.50	4.52	4.34	4.02	5.36	4.22	4.26
					Ovarian Cancer					
IGROV1	4.59	<4.00	5.64	4.57	4.51	4.20	<4.00	5.07	4.24	4.25
OVCAR-3	4.44	4.55	7.19	4.55	4.49	4.14	<4.00	5.54	4.24	4.24
OVCAR-4	4.05	<4.00	5.29	4.56	4.30	<4.00	<4.00	<4.00	4.25	<4.00
OVCAR-5	4.45	4.18	5.10	4.56	4.51	<4.00	<4.00	4.11	4.26	4.26
OVCAR-8	4.48	<4.00	5.63	4.59	4.49	<4.00	<4.00	<4.00	4.09	4.24
SK-OV-3	4.45	<4.00	5.79	4.46	4.48	<4.00	<4.00	5.07	4.19	4.21
					Renal Cancer					
786–0	4.74	4.49	5.73	4.64	4.40	4.26	<4.00	5.34	4.32	4.20
A498	4.57	4.38	5.87	4.40	4.52	4.19	<4.00	5.40	4.14	4.25
ACHN	5.14	4.65	5.74	4.63	4.54	4.46	<4.00	5.36	4.27	4.27
CAKI-1	4.45	5.06	5.70	4.75	4.46	4.15	<4.00	5.29	4.31	4.23
RXF 393	4.52	4.42	5.50	4.56	4.51	<4.00	<4.00	<4.00	4.20	4.25
SN12C	5.20	4.72	5.68	4.69	4.53	4.50	<4.00	<4.00	4.25	4.26
TK-10	4.43	4.06	5.61	4.47	4.52	4.18	<4.00	5.18	4.23	4.26
UO-31	4.57	<4.00	5.65	4.55	4.48	4.25	<4.00	5.21	4.27	4.22
					Prostate Cancer					
PC-3	4.54	4.35	5.59	4.59	4.51	<4.00	<4.00	<4.00	4.27	4.25
DU-145	4.42	4.76	4.94	4.52	4.50	<4.00	4.38	5.37	4.19	4.25
					Breast Cancer					
MCF7	<4.00	4.90	5.84	<4.00	4.40	<4.00	4.40	5.26	<4.00	4.14
NCI/ADR-RES	4.49	4.46	7.24	4.50	4.50	<4.00	<4.00	5.00	4.13	4.25
MDA-MB-31/ATCC	4.99	4.76	6.13	4.63	4.49	4.23	<4.00	5.51	4.22	4.21
HS 578T	4.46	4.19	5.57	4.22	4.28	<4.00	<4.00	<4.00	<4.00	<4.00
MDA-MB-435	4.51	4.94	7.68	4.70	4.52	4.23	4.02	<4.00	4.30	4.26
BT-549	4.19	4.23	5.69	4.39	4.24	<4.00	<4.00	5.20	4.07	<4.00
T-47D	<4.00	4.31	5.34	4.30	4.12	<4.00	<4.00	<4.00	<4.00	<4.00
MG_MID[e]	4.5	4.53	5.87	4.57	4.42	4.11	4.12	5.2	4.21	4.16

[a] Data obtained from NCI's in vitro disease-oriented tumor cells screen. [b] pTGI is the −log of the molar concentration giving total growth inhibition. [c] pLC$_{50}$ is the −log of the molar concentration leading to 50% net cell death. [d] ND: not determined. [e] MG_MID (mean graph midpoint) is the arithmetical mean value for all tested cancer cell lines. If the indicated effect was not attainable within the used concentration interval, the highest tested concentration was used for the calculation.

indicating an orientation of the transition dipole of the molecule perpendicular to the long axis of the binding pocket.[14–16]

Linear Dichroism. By measuring the flow linear dichroism of the different drug−nucleic acid complexes, it was possible to elucidate the binding geometry of **4c** bound to DNA.[17,18] Figure 6 (lower panel) shows absorbance, LD, and reduced LD (LD$_r$) spectra for **4c** at different [drug]/[DNA] ratios. Examination of the figures revealed that the LD spectra of **4c** complexed

Table 5. Effect of Isoindolo[2,1-*a*]quinoxalines **4a–e** against Different Drug-Resistant Cell Lines

	growth inhibition (GI_{50}) [μM][a]		
cpd	MCF-7^{wt}	MCF-7^{MDR}	RI[b]
4a	6.5 ± 0.7	10.6 ± 1.4	1.6
4b	3.7 ± 0.4	8.1 ± 1.2	2.2
4c	0.17 ± 0.02	0.15 ± 0.02	0.9
4d	5.1 ± 0.5	9.2 ± 0.8	1.8
4e	3.3 ± 0.2	7.6 ± 0.6	2.3
cpd	CEM^{wt}	CEM$^{Vbl-100}$	RI[b]
4a	4.7 ± 0.5	3.8 ± 0.4	0.80
4b	2.9 ± 0.3	3.0 ± 0,3	1.04
4c	0.02 ± 0.002	0.02 ± 0.002	1.0
4d	15.5 ± 1.6	15.1 ± 1.6	0.97
4e	2.2 ± 0.31	1.9 ± 0.2	0.86
cpd	LoVo^{wt}	LoVo^{Doxo}	RI[b]
4a	ND[c]	ND	ND
4b	ND	ND	ND
4c	0.13 ± 0.013	0.13 ± 0.02	1.0
4d	ND	ND	ND
4e	ND	ND	ND

[a] Concentration causing 50% growth inhibition of tumor cells determined by MTT test after 72 h of incubation. Data represented as mean ± SEM of three independent experiments. [b] RI: resistance index. [c] ND: not determined.

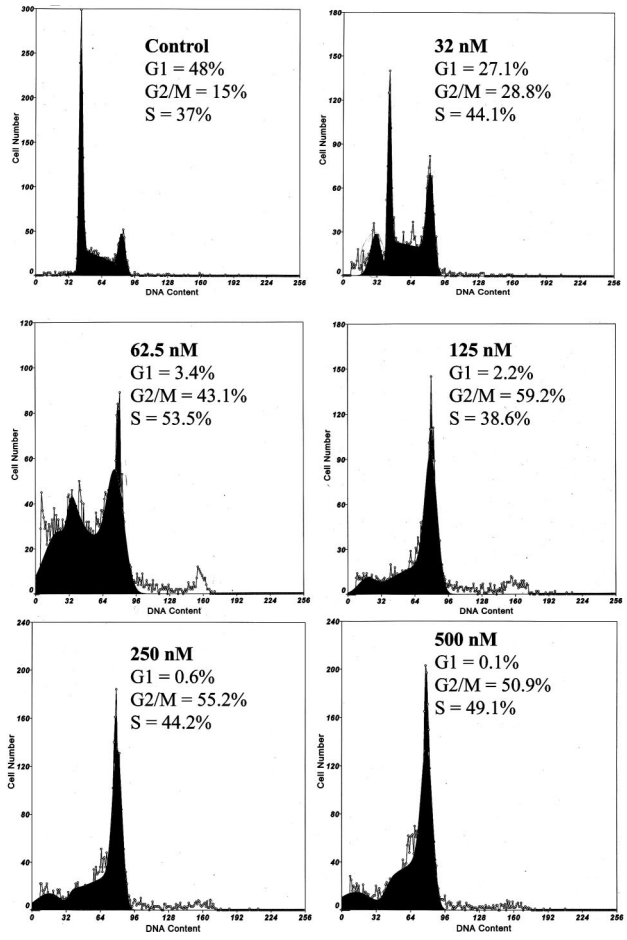

Figure 1. Histograms of flow cytometry data of Jurkat cells treated at the indicated concentrations of **4c**. After 24 h of treatment, cells were labeled with propidium iodide and analyzed by flow cytometry as described in the Experimental Section.

with DNA were negative in the 230−300 nm region where DNA absorbed. A significant increase in the values of LD of the DNA band at 260 nm for these drug−DNA complexes was observed,

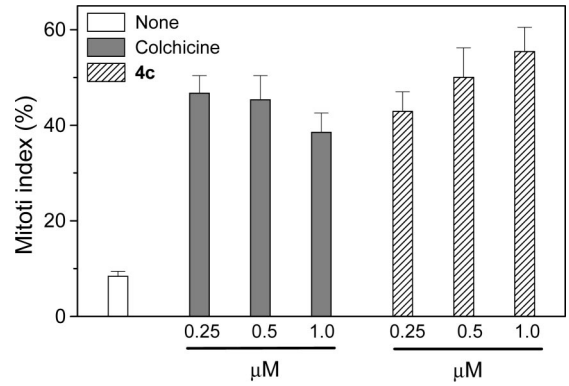

Figure 2. Mitotic index determinations. Jurkat cells were treated with **4c** at the indicated concentrations. A total of 400 cells/treatment was scored for the presence of mitotic figures by contrast phase microscopy, and the mitotic index was calculated as the proportion of cells with mitotic figures. Colchicine was used as reference compound. Data are expressed as mean ± SEM of three independent experiments.

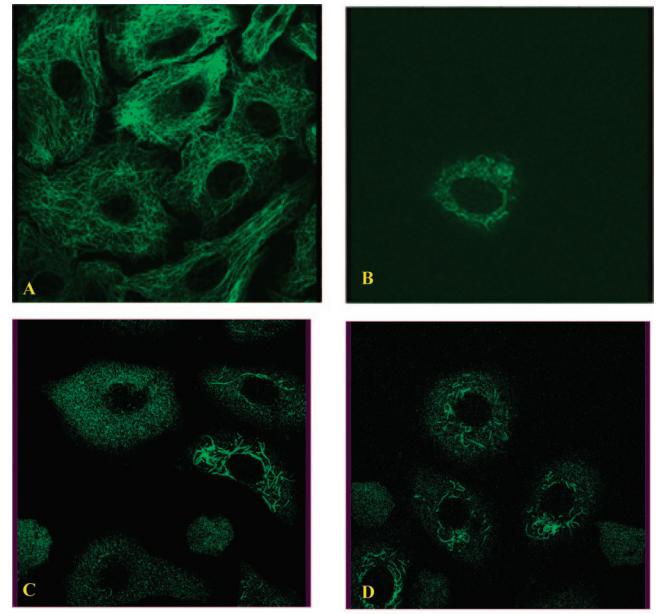

Figure 3. Immunofluorescences images of A-549 cells treated with anti-β-tubulin antibody and with a secondary antibody tetramethyl rhodamine isothiocyanate (TRITC)-conjugated and then observed by confocal microscopy (panel A). Cells were exposed to concentrations of 5 μM (panel C) and 2.5 μM (panel D) of compound **4c** for 24 h. As reference, vinblastine (panel B) at the concentration of 1 μM was used.

suggesting that the DNA became better oriented in the hydrodynamic field because of a stiffening of the helix upon binding of the drug.[17] The negative LD signals in the long-wavelength absorption (S_0-S_1 transition, 300−450 nm) of **4c** revealed that it was oriented perpendicularly to the flow field, usually caused by an intercalation into the DNA helix. This assumption was further corroborated by the observation that the intensity of the DNA signal increased on addition of the drug.

The LD_r spectrum provided further information on the average orientation of the transition moment of the dye relative to those of the DNA bases and allowed us to distinguish between homogeneous and heterogeneous binding. A nearly constant value of LD_r over the range 310−400 nm was observed (Figure 6, lower panel), which unambiguously proved an almost exclusive intercalation of **4c** into the DNA.

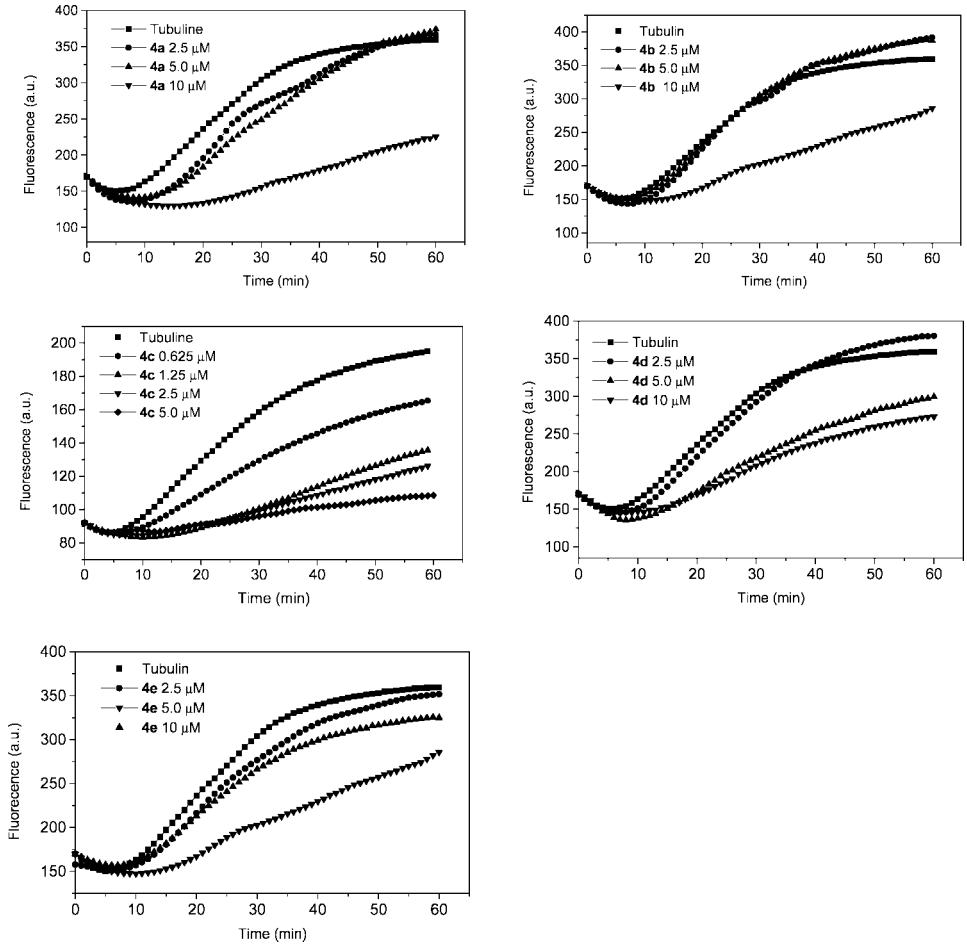

Figure 4. Effects of compound **4c** on microtubule assembly. Purified tubulin was incubated in the absence or in the presence of the compound at the indicated concentrations. Fluorescence measurement (λ_{ex} = 355 nm and λ_{em}= 450 nm) was determined every minute for 60 min at 37 °C. Polymerization was initiated by the addition of tubulin.

Topoisomerases Assay. DNA relaxation experiments were performed with both topoisomerase I and II. Supercoiled plasmid pBR322 was incubated with human topoisomerase I and **4a-e** in concentrations ranging from 0.5 to 200 μM. The unwinding of the plasmid was monitored by agarose gel electrophoresis. For compound **4c**, the picture of the gel (Figure 7, panel A3) indicated that at low concentrations, the intensity of the slowest migrating band (corresponding to nicked + fully relaxed DNA) increased significantly, whereas at higher concentrations, the relaxation of DNA was inhibited, as observed with the reference topoisomerase I poison camptothecin used at a concentration of 20 μM. To exclude a nonspecific effect due to a direct interaction of **4c** with DNA, the relaxation assay was repeated on ethidium bromide containing agarose gel, as shown in Figure 7, panel B3. Under these conditions, the presence of nicked DNA molecules was observed, indicating that compound **4c** may stimulate DNA cleavage by topoisomerase I.

As compared to compound **4c**, the other derivatives **4a**, **b**, **d**, and **e** exhibited a less pronounced influence on the topoisomerase activity (Figure 7, panels A1 and A2). The topoisomerase-induced relaxation was inhibited only at relatively high concentrations. Moreover, the analysis of the relaxation assay with an ethidium bromide-containing agarose gel revealed that over the whole concentration range of compounds **4a**, **b**, **d**, and **e** (1−200 μM), a small and insignificant amount of single strand breaks were formed, suggesting that these derivatives did not efficiently stabilize the topoisomerase cleavage complex but acted only as catalytic topoisomerase I inhibitors.

Analogous experiments were performed with human topoisomerase II, and the results indicated no effect of isoindolo[2,1-*a*]quinoxaline **4a**−**e** on this enzyme (data not shown).

Loss of Plasma Membrane Asymmetry during Apoptosis. To better characterize drug-induced apoptosis, a biparametric cytofluorimetric analysis, using propidium iodide (PI) and AnnexinV-fluorescein isothiocyanate (FITC) which stain DNA and phosphatidylserine (PS) residues, was performed.[19] Because externalization of PS occurs in the first stages of apoptosis, Annexin-V staining identifies apoptosis at an earlier stage than sub-G_1 appearance, which represents a later event of apoptosis as a consequence of nuclear changes such as DNA fragmentation. After drug treatment for 24 h, Jurkat cells were labeled with the two dyes and washed, and the resulting red (PI) and green (FITC) fluorescence was monitored by flow cytometry. It can be observed from Figure 8 that **4c** provoked a significant induction of apoptotic cells in a concentration-dependent manner after 24 h of treatment. These findings prompted us to further investigate the apoptotic machinery after treatment with the test compound.

Variations of the Mitochondrial Potential. Mitochondria play an essential role in the propagation of apoptosis.[20,21] It is well established that, at an early stage, apoptotic stimuli alter the mitochondrial transmembrane potential ($\Delta\psi_{mt}$). To address whether **4c** affected the $\Delta\psi_{mt}$, it was monitored by fluorescence of the dye 5,5′,6,6′-tetrachloro-1,1′,3,3′-tetraethylbenzimidazolcarbocyanine (JC-1), which is considered as a reliable probe to assess $\Delta\psi_{mt}$.[22] JC-1 has the unique property of forming red

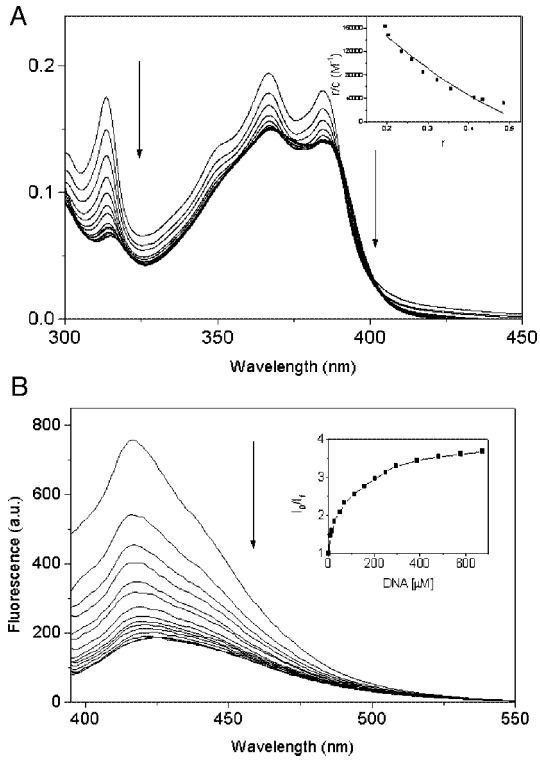

Figure 5. Spectrophotometric titration (A) of st-DNA to **4c** in ETN buffer (0.01 M, pH = 7.0, T = 25 °C). The Scatchard plot of the spectrophotometric titration is presented in the inset. The solid lines represent the best fit of the McGhee and von Hippel equation to the experimental data. Fluorometric titration (B) of st-DNA to **4c** in ETN buffer (0.01 M, pH = 7.0, T = 25 °C). The Stern−Volmer plot is presented in the inset.

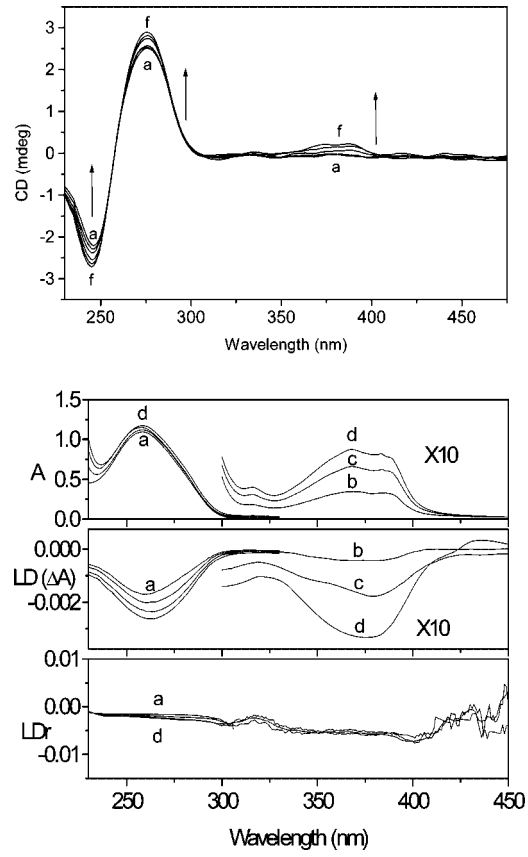

Figure 6. Upper panel: circular dichroism spectra of **4c** complexed to st-DNA at different [dye]/[DNA] ratios from *a* to *f* (*a* = 0.00, *b* = 0.02, *c* = 0.04, *d* = 0.08, *e* = 0.2, and *f* = 0.4) in ETN buffer (0.01 M, pH = 7.0, T = 25 °C). Lower panel: absorbance *A*, linear dichroism LD, and reduced linear dichroism LD_r spectra of mixtures of st-DNA and **4c** at different [drug]/[DNA] ratios (*a* = 0.00, *b* = 0.04, *c* = 0.08, and *d* = 0.2) in ETN buffer (0.01 M, pH = 7.0).

fluorescent aggregates locally and spontaneously under high mitochondrial $\Delta\psi_{mt}$, whereas the monomeric form fluoresces in green. Treated Jurkat cells in the presence of **4c** exhibited a dramatic shift in fluorescence in a dose-dependent manner compared to the control cells, indicating depolarization of mitochondrial membrane potential. The percentage of cells with low mitochondrial potential for **4c** is depicted in Figure 9 (upper panel). It is interesting to note that the disruption of $\Delta\psi_{mt}$ is associated with the appearance of Annexin-V positivity in the treated cells. As a matter of fact, the dissipation of $\Delta\psi_{mt}$ is characteristic of apoptosis and has commonly been observed with a variety of anticancer drugs, irrespective of the cell type.

Mitochondrial Generation of Reactive Oxygen Species (ROS). Mitochondrial membrane depolarization is associated with mitochondrial production of ROS.[23] It was therefore investigated whether ROS production had increased after treatment with the test compound. The probe hydrohethidine (HE), the fluorescence of which appears if ROS are generated,[24] was utilized in order to investigate the effects of the test compound on the production of oxygen species during apoptosis. HE is oxidized by superoxide anion into an ethidium ion, which emits red fluorescence. Superoxide is produced by mitochondria because of a shift from the normal 4-electron reduction of O_2 to a 1-electron reduction when cytochrome C is released from mitochondria. The results presented in Figure 9 (middle panel) show that **4c** significantly induced the production of ROS in comparison to the control cells.

Moreover, the damage produced by ROS in mitochondria by assessing the oxidation state of cardiolipin, a phospholipid restricted to the inner mitochondrial membrane, was evaluated by using the specific dye NAO.[25] This fluorescent probe specifically binds to cardiolipin, and its binding affinity and fluorescence properties depend on the oxidation state of cardiolipin. NAO binds with high affinity to a non-oxidized cardiolipin in a 2:1 ratio, whereas in the case of oxidized cardiolipin, NAO has been reported to bind this phospholipid with a decreased affinity reflected by a lower fluorescence intensity.[26] Therefore, oxidative stress localized in mitochondria can be assessed by measuring the fluorescence of NAO. Jurkat treated cells showed (Figure 9, lower panel) a progressive and remarkable decrease in mean NAO fluorescence with increasing concentration of **4c**,consistent with a loss in cardiolipin content.

Caspase Activation. The role of the caspases in apoptosis induction was also studied. In fact, programmed cell death is associated with activation of this large family of proteases.[27,28] Caspases are synthesized as proenzymes activated by cleavage. Caspase-8 and caspase-9, called apical caspases, are usually the first to be stimulated in the apoptotic process, and then, they activate effector caspases such as caspase-3.

Among the apical caspases, caspase-9 is activated in response to DNA damage, whereas caspase-8 is one effector of the death receptor Fas (CD95, APO-1).[29] Caspase-3, in particular, is essential to the propagation of the apoptotic signal after the exposure to many DNA-damaging agents and anticancer drugs, and in many cases, its activation is associated with a dissipation of the mitochondrial potential.[30,31]

The results showed that compound **4c** was able to induce the activation of caspase-3 and in particular caspase-9. A modest activity of caspase-8 was also recorded, suggesting that the

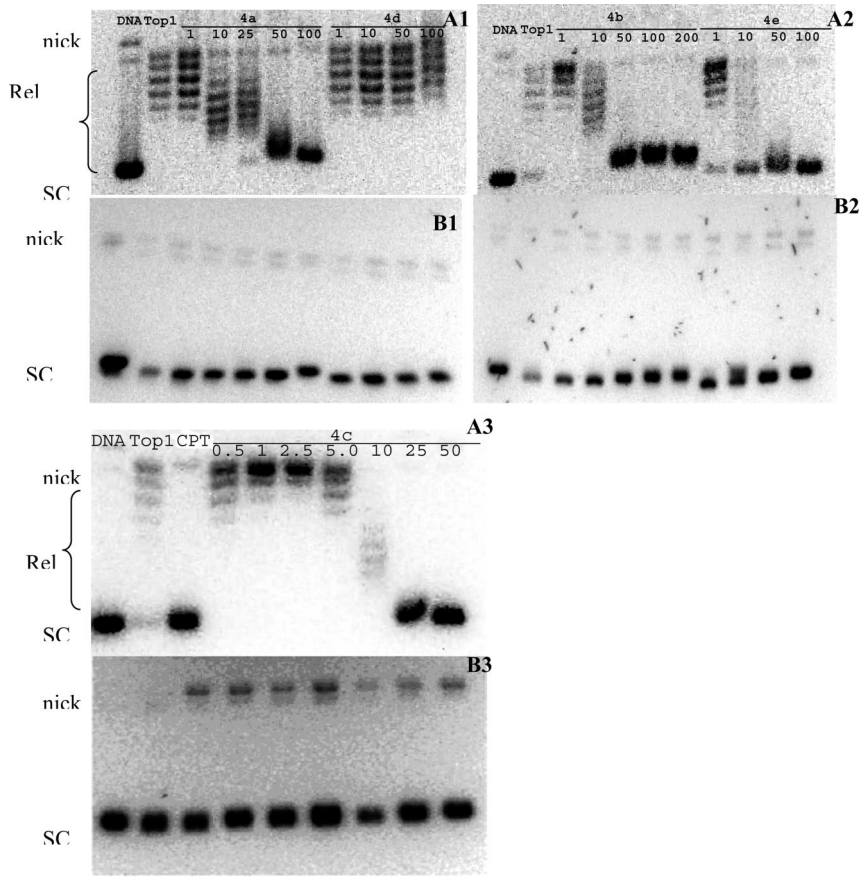

Figure 7. Effect of increasing concentrations of compounds **4a**−**e** on the relaxation of pBR322 plasmid DNA by human topoisomerase I. Supercoiled pBR322 DNA was incubated with five units of topoisomerase I in the absence or in the presence of the indicated concentrations of compounds **4a**−**e** expressed in μM. Camptothecin was used as reference compound at a concentration of 20 μM. DNA samples were separated by electrophoresis on agarose gel without (panels A1, A2, and A3) or with (panels B1, B2, and B3) ethidium bromide. Sc, supercoiled; Rel, relaxed; Nick, nicked.

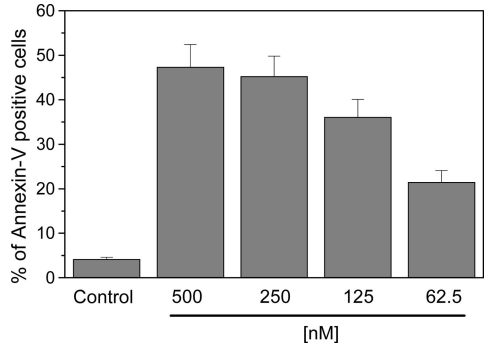

Figure 8. Percentage of Annexin-V positive cells after 24 h of incubation at the indicated concentrations of compound **4c**. Data are expressed as mean ± SEM of three independent experiments.

action of the test compound is integrated at the mitochondrial level (Figure 10).

Conclusion

The present results show that isoindolo[2,1-*a*]quinoxaline derivatives, obtained in very good yields with a straightforward synthesis, exhibit high cytotoxic activity against a very wide range of human tumor cell lines with GI_{50} values reaching nanomolar concentrations. More importantly, these compounds are also found to be active in cells overexpressing P-gp, suggesting that these derivatives might be useful in treating drug-refractory patients. At the molecular level, such compounds act through inhibition of tubulin polymerization and topoisomerase I activity.

In our cell cycle study, cells treated with **4c** accumulated in G2-M phase with concomitant loss of the G1 phase. By using in vitro tubulin polymerization assay, it was found that **4c** inhibited tubulin polymerization in a concentration-dependent manner, in a way similar to colchicine and vinblastine, indicating that these compounds can be classified as microtubule depolymerizing agents. Moreover, the mitotic index determinations and the immunofluorescence studies clearly confirmed the interaction with tubulin. It is interesting to note that, to the best of our knowledge, the structure of isoindolo[2,1-*a*]quinoxaline derivatives does not resemble any of the known antimitotic drugs.

The spectrophotometric results indicate that **4c** bound to DNA by intercalation, and consequently, the macromolecule may be considered as a potential target for this class of compounds.

Many reports showed that DNA intercalators could be topoisomerase I and/or topoisomerase II inhibitors.[32,33] By using a DNA relaxation assay, it was determined that compound **4c** inhibited topoisomerase I catalytic activity but not topoisomerase II activity.

Further studies show that **4c** is a potent inducer of apoptosis in Jurkat cell line. The induction of apoptosis is associated with (i) dissipation of the mitochondrial transmembrane potential, (ii) production of reactive oxygen species and cardiolipin oxidation, and (iii) activation of caspase-3 and caspase-9. All of these effects are associated with both antimitotic drugs and topoisomerase I inhibitors.[34–37]

In conclusion, these results, in their whole, suggest that isoindolo[2,1-*a*]quinoxaline derivative **4c** acts on both tubulin and

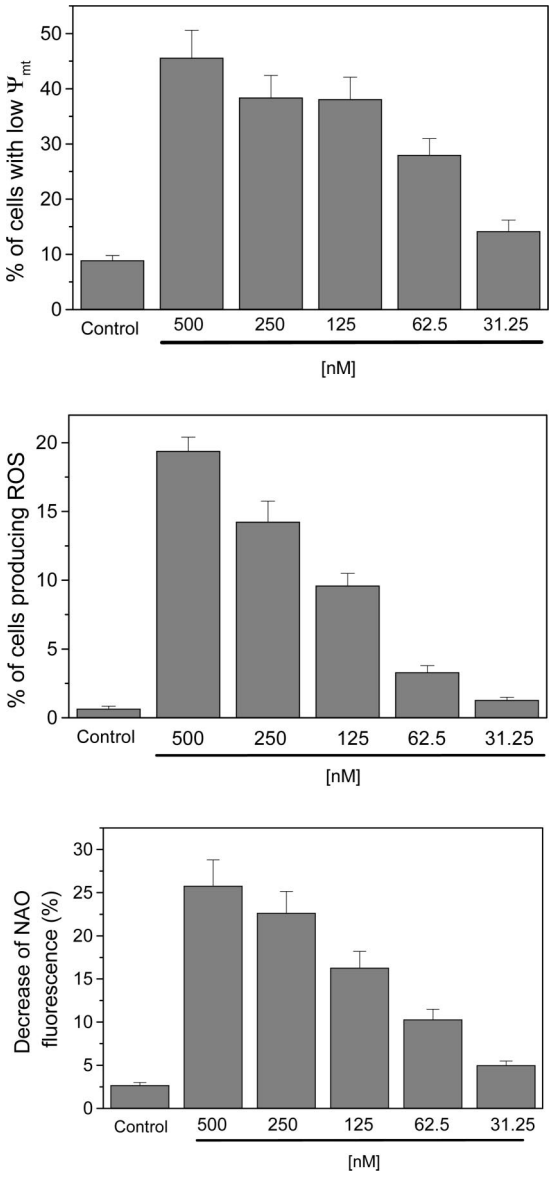

Figure 9. Assessment of mitochondrial dysfunction after treatment with compound **4c**. Upper panel: induction of loss of mitochondrial membrane potential after 24 h of incubation of Jurkat cells by **4c** at the indicated concentrations. Cells were stained with the fluorescent probe JC-1 and analyzed by flow cytometry. Middle panel: mitochondrial production of ROS in Jurkat cells. After 24 h of incubation with **4c**, cells were stained with HE and analyzed by flow cytometry. Lower panel: decrease of mean fluorescence intensity of the cardiolipin-binding dye 10-*N*-nonyl-acridine orange (NAO) in Jurkat cells after treatment for 24 h with **4c** at the indicated concentrations and analyzed by flow cytometry. Data are expressed as mean ± SEM of three independent experiments.

topoisomerase I. Considering their interesting biochemical mechanism of action and the potent activity against a very wide range of human cell lines, these new derivatives deserve further investigations as promising antitumor agents. In particular, it will be interesting to determine whether tubulin or topoisomerase I is the principal target of isoindolo[2,1-*a*]quinoxaline in tumor cells.

Experimental Section

Chemistry. All melting points were taken on a Buchi-Tottoli capillary apparatus and are uncorrected; IR spectra were determined in bromoform with a Jasco FT/IR 5300 spectrophotometer; ^{1}H and ^{13}C NMR spectra were measured at 200 and 50.3 MHz, respectively, by using a Bruker AC series 200 MHz spectrometer (TMS as internal reference). Column chromatography was performed with Merck silica gel 230−400 mesh ASTM or with Sepacore Buchi apparatus. Elemental analyses were within ±0.4% of the theoretical values and were performed with a VARIO EL III elemental analyzer.

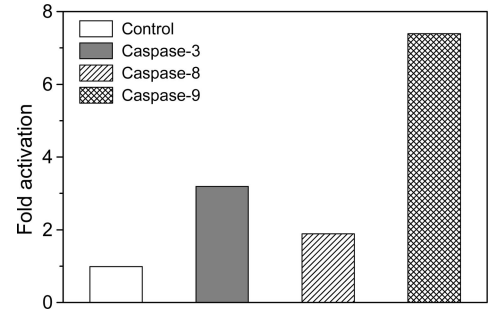

Figure 10. Caspase activity induced by compound **4c**. Jurkat cells were incubated in the presence of **4c** at a concentration of 500 nM. After 24 h of treatment, cells were harvested and assayed for caspase-3, caspase-8, and caspase-9 activity by using the cell-permeable substrates for caspase-3 (FITC-DEVD-fmk), caspase-8 (FITC-IETD-fmk), and caspase-9 (FITC-LEDH-fmk). After 1 h of incubation at 37 °C, the cells were washed and analyzed by flow cytometry. Data are represented as fold increase of enzymes activity, in comparison to the control.

Synthesis of Substituted 1-Cyano-2-(2′-aminophenyl)isoindoles 3a–e. To a solution of sodium hydrogen sulfite (1.56 g, 0.015 mol) in water (38 mL), phthalaldehyde **2** (2 g, 0.015 mol) was added. The mixture was stirred until the solid was dissolved, and the appropriate 1,2-phenylenediamine **1a**−**d** (0.015 mol) was added. The reaction was heated on a steam bath for 30 min, then KCN (3.39 g, 0.052 mol) in water (8.0 mL) was added, and the mixture was heated for an additional 90 min. The solid formed upon cooling was filtered and purified by chromatography. In the case of derivative **3e**, the 1,2-phenylenediamine **1e** was first dissolved in DMF (15 mL) and then added to the reaction mixture.

1-Cyano-2-(2′-aminophenyl)isoindole 3a. This compound was purified by flash chromatography by using dichloromethane as eluent to give a solid: yield 65%; mp 150−151 °C; IR 3473, 3363 (NH_2), 2202 (CN) cm^{-1}; ^{1}H NMR (DMSO-d_6) δ 5.19 (s, 2H, NH_2), 6.70 (t, 1H, J = 7.2 Hz, H-5′), 6.94 (d, 1H, J = 7.2 Hz, H-3′), 7.15−7.19 (m, 3H, H-4′, H-5, H-6′), 7.31 (t, 1H, J = 8.2 Hz, H-6), 7.66 (d, 1H, J = 8.2 Hz, H-4), 7.78 (d, 1H, J = 8.2 Hz, H-7), 7.86 (s, 1H, H-3); ^{13}C NMR (DMSO-d_6) δ 93.9 (s), 114.0 (s), 115.8 (d), 116.1 (d), 117.5 (d), 121.5 (d), 122.2 (d), 122.4 (d), 122.5 (s), 124.1 (s), 125.5 (d), 127.8 (d), 130.4 (d), 131.2 (s), 144.1 (s). Anal. ($C_{15}H_{11}N_3$) C, H, N.

1-Cyano-2-(2′-amino-3′-methylphenyl)isoindole 3b. This compound was purified by a Sepacore Buchi apparatus by using dichloromethane:cyclohexane (7:3) as eluent to give compound **3b**: yield 40%; mp 62−63 °C; IR 3481, 3388 (NH_2), 2200 (CN) cm^{-1}; ^{1}H NMR ($CDCl_3$) δ 2.25 (s, 3H, CH_3), 3.55 (s, 2H, NH_2), 6.80 (t, 1H, J = 7.6 Hz, H-5′), 7.10 (d, 1H, J = 7.6 Hz, H-6′), 7.14 (d, 1H, J = 7.6 Hz, H-4′), 7.23 (t, 1H, J = 8.1 Hz, H-5), 7.31 (t, 1H, J = 8.1 Hz, H-6), 7.44 (s, 1H, H-3), 7.69 (d, 1H, J = 8.1 Hz, H-4), 7.73 (d, 1H, J = 8.1 Hz, H-7); ^{13}C NMR ($CDCl_3$) δ 17.6 (q), 92.2 (s), 113.0 (s), 117.9 (d), 118.3 (d), 120.5 (d), 120.9 (d), 123.2 (d), 123.8 (s), 124.1 (s), 124.6 (s), 125.5 (d), 125.9 (d), 131.8 (s), 131.9 (d), 140.5 (s). Anal. ($C_{16}H_{13}N_3$) C, H, N.

Further elution gave 1-cyano-2-(2′-amino-6′-methylphenyl)isoindole: yield 45%; mp 87−88 °C; IR 3483, 3390 (NH_2), 2202 (CN) cm^{-1}; ^{1}H NMR ($CDCl_3$) δ 1.98 (s, 3H, CH_3), 3.45 (s, 2H, NH_2), 6.69 (d, 1H, J = 8.1 Hz, H-3′), 6.75 (d, 1H, J = 8.1 Hz, H-5′), 7.16 (t, 1H, J = 8.1 Hz, H-4′), 7.20 (t, 1H, J = 7.6 Hz, H-5), 7.26 (t, 1H, J = 7.6 Hz, H-6), 7.35 (s, 1H, H-3), 7.71 (d, 1H, J = 7.6 Hz, H-4), 7.74 (d, 1H, J = 7.6 Hz, H-7); ^{13}C NMR ($CDCl_3$) δ 17.0 (q), 94.7 (s), 113.6 (s), 114.1 (d), 118.5 (d), 120.0 (d), 120.3 (d), 121.0 (d), 123.2 (d), 123.6 (s), 124.8 (s), 125.9 (d), 130.3 (s), 130.6 (d), 136.3 (s), 143.0 (s). Anal. ($C_{16}H_{13}N_3$) C, H, N.

1-Cyano-2-(2′-amino-4′-methoxyphenyl)isoindole 3c. This compound was purified by flash chromatography by using dichloromethane as eluent to give a solid: yield 95%; mp 116−117 °C; IR 3465, 3375 (NH_2), 2198 (CN) cm^{-1}; ^1H NMR ($CDCl_3$) δ 3.64 (bs, 2H, NH_2), 3.80 (s, 3H, CH_3), 6.38 (bs, 1H, H-3′), 6.42 (d, 1H, J = 7.9 Hz, H-5′), 7.12 (d, 1H, J = 7.9 Hz, H-6′), 7.14 (t, 1H, J = 8.6 Hz, H-5), 7.29 (t, 1H, J = 8.6 Hz, H-6), 7.41 (s, 1H, H-3), 7.66 (d, 1H, J = 8.6 Hz, H-4), 7.70 (d, 1H, J = 8.6 Hz, H-7); ^{13}C NMR ($CDCl_3$) δ 55.4 (q), 95.4 (s), 101.4 (d), 104.5 (d), 113.9 (s), 117.5 (s), 118.2 (d), 120.8 (d x 2), 123.1 (d), 124.5 (s), 125.8 (d), 128.7 (d), 131.7 (s), 143.3 (s), 161.5 (s). Anal. ($C_{16}H_{13}N_3O$) C, H, N.

1-Cyano-2-(2′-amino-4′,5′-dimethylphenyl)isoindole 3d. This compound was purified by flash chromatography by using dichloromethane as eluent to give a solid: yield 85%; mp 119−120 °C; IR 3465, 3375 (NH_2), 2202 (CN) cm^{-1}; ^1H NMR ($CDCl_3$) δ 2.17 (s, 3H, CH_3), 2.22 (s, 3H, CH_3), 3.44 (s, 2H, NH_2), 6.64 (s, 1H, H-3′), 6.95 (s, 1H, H-6′), 7.12 (t, 1H, J = 7.6 Hz, H-5), 7.27 (t, 1H, J = 7.6 Hz, H-6), 7.38 (s, 1H, H-3), 7.64 (d, 1H, J = 7.6 Hz, H-4), 7.68 (d, 1H, J = 7.6 Hz, H-7); ^{13}C NMR ($CDCl_3$) δ 18.6 (q), 19.7 (q), 95.1 (s), 114.0 (s), 118.1 (d), 118.2 (d), 120.6 (d), 120.9 (d), 121.8 (s), 123.1 (d), 124.5 (s), 125.8 (d), 127.0 (s), 128.2 (d), 131.7 (s), 139.6 (s), 139.7 (s). Anal. ($C_{17}H_{15}N_3$) C, H, N.

1-Cyano-2-(2′-amino-4′,5′-dichlorophenyl)isoindole 3e. This compound was purified by flash chromatography by using dichloromethane as eluent to give a solid: yield 77%; mp 71−72 °C; IR 3394, 3340 (NH_2), 2200 (CN) cm^{-1}; ^1H NMR (DMSO-d_6) δ 5.75 (2H, s, NH_2), 7.12 (1H, s, H-3′), 7.16 (1H, t, J = 8.4 Hz, H-5), 7.32 (1H, t, J = 8.4 Hz, H-6), 7.58 (1H, s, H-6′), 7.66 (1H, d, J = 8.4 Hz, H-4), 7.78 (1H, d, J = 8.4 Hz, H-7), 7.91 (1H, s, H-3); ^{13}C NMR (DMSO-d_6) δ 94.0 (s), 113.8 (s), 115.8 (s), 116.2 (d), 117.5 (d), 121.6 (d), 121.7 (s), 122.4 (d), 122.6 (d), 124.2 (s), 125.8 (d), 129.6 (d), 131.2 (s), 132.9 (s), 144.7 (s). Anal. ($C_{15}H_9Cl_2N_3$) C, H, N.

General Procedure for the Synthesis of 5*H*-Isoindolo[2,1-*a*]quinoxalin-6-ones 4a–e. 1-Cyano-2-(2′-aminophenyl)isoindoles **3a–e** (3 mmol) were dissolved in acetic acid (10 mL) and refluxed for 30 min. The reaction mixture was poured into ice water (150 mL). The resulting precipitate was collected by filtration and recrystallized from ethanol.

5*H*-Isoindolo[2,1-*a*]quinoxalin-6-one 4a. Yield 99%; mp 255−256 °C; IR 3390, 3203 (NH), 1685 (CO) cm^{-1}; ^1H NMR (DMSO-d_6) δ 7.75 (dt, 1H, J = 7.0, 1.6 Hz, H-2), 7.78−7.91 (m, 2H, H-3 and H-4), 7.93 (s, 1H, H-11), 7.96 (t, 1H, J = 7.8 Hz, H-9), 8.00 (t, 1H, J = 7.8 Hz, H-8), 8.27 (dd, 1H, J = 7.0, 1.6 Hz, H-1), 8.34 (d, 1H, J = 7.8 Hz, H-10), 8.84 (d, 1H, J = 7.8 Hz, H-7), 12.35 (bs, 1H, NH);^{13}C NMR (DMSO-d_6) δ 124.1 (d), 127.0 (d), 127.5 (d), 127.8 (d), 127.9 (d), 128.9 (d), 130.9 (d), 131.4 (d), 133.1 (s), 133.4 (d), 135.3 (s), 138.9 (s), 141.0 (s), 143.9 (s), 161.7 (s). Anal. ($C_{15}H_{10}N_2O$) C, H, N.

4-Methyl-5*H*-isoindolo[2,1-*a*]quinoxalin-6-one 4b. Yield 98%; mp 338−339 °C; IR 3360, 3284 (NH), 1632 (CO) cm^{-1}; ^1H NMR (DMSO-d_6) δ 2.62 (s, 3H, CH_3), 7.32−7.40 (m, 2H, H-9 and H-3), 7.45 (t, 1H, J = 6.8 Hz, H-2), 7.51 (t, 1H, J = 8.8 Hz, H-8), 7.96 (d, 1H, J = 8.8 Hz, H-10), 8.27 (d, 1H, J = 6.8 Hz, H-1), 8.47 (d, 1H, J = 8.8 Hz, H-7), 9.24 (s, 1H, H-11), 12.53 (bs, 1H, NH);^{13}C NMR (DMSO-d_6) δ 17.8 (q), 104.8 (s), 114.8 (d), 117.3 (d), 119.2 (d), 121.5 (d), 122.3 (s), 125.0 (d), 125.1 (s), 125.2 (d), 125.3 (s), 127.1 (d), 127.3 (s x 2), 130.0 (d), 147.0 (s). Anal. ($C_{16}H_{12}N_2O$) C, H, N.

3-Methoxy-5*H*-isoindolo[2,1-*a*]quinoxalin-6-one 4c. Yield 75%; mp 293−294 °C; IR 3363, 3280 (NH), 1635 (CO) cm^{-1}; ^1H NMR (DMSO-d_6) δ 3.84 (3H, s, CH_3), 7.04 (s, 1H, H-4), 7.05 (d, 1H, J = 9.8 Hz, H-2), 7.40 (t, 1H, J = 7.8 Hz, H-9), 7.51 (t, 1H, J = 7.8 Hz, H-8), 7.95 (d, 1H, J = 7.8 Hz, H-10), 8.36 (d, 1H, J = 9.8 Hz, H-1), 8.51 (d, 1H, J = 7.8 Hz, H-7), 9.18 (s, 1H, H-11), 13.50 (bs, 1H, NH);^{13}C NMR (DMSO-d_6) δ 55.7 (q), 101.5 (d), 104.6 (s), 112.7 (d), 115.7 (d), 116.2 (s), 118.2 (d), 119.1 (d), 120.9 (d), 124.3 (d), 124.4 (s), 126.2 (d), 126.6 (s), 128.5 (s), 147.1 (s), 158.9 (s). Anal. ($C_{16}H_{12}N_2O_2$) C, H, N.

2,3-Dimethyl-5*H*-isoindolo[2,1-*a*]quinoxalin-6-one 4d. Yield 96%; mp 370−371 °C; IR 3365, 3286 (NH), 1631 (CO) cm^{-1}; ^1H NMR (DMSO-d_6) δ 2.30 (3H, s, CH_3), 2.35 (3H, s, CH_3), 7.31 (s, 1H, H-4), 7.46 (t, 1H, J = 7.8 Hz, H-9), 7.57 (t, 1H, J = 7.8 Hz, H-8), 8.00 (d, 1H, J = 7.8 Hz, H-10), 8.09 (s, 1H, H-1), 8.41 (d, 1H, J = 7.8 Hz, H-7), 9.02 (s, 1H, H-11), 13.14 (bs, 1H, NH);^{13}C NMR (DMSO-d_6) δ 19.5 (q), 19.6 (q), 116.7 (d), 117.4 (d), 118.7 (s), 119.1 (d), 119.6 (d), 121.0 (s), 122.0 (d), 125.3 (s), 125.4 (d), 125.8 (s), 127.6 (d), 127.9 (s), 135.9 (s), 139.0 (s), 147.2 (s). Anal. ($C_{17}H_{14}N_2O$) C, H, N.

2,3-Dichloro-5*H*-isoindolo[2,1-*a*]quinoxalin-6-one 4e. Yield 87%; mp 340−343 °C; IR 3350, 3302 (NH), 1645 (CO) cm^{-1}; ^1H NMR (DMSO-d_6) δ 7.43 (t, 1H, J = 7.8 Hz, H-9), 7.54 (t, 1H, J = 7.8 Hz, H-8), 7.86 (s, 1H, H-4), 7.95 (d, 1H, J = 7.8 Hz, H-10), 8.52 (d, 1H, J = 7.8 Hz, H-7), 8.85 (s, 1H, H-1), 9.32 (s, 1H, H-11), 12.46 (bs, 1H, NH);^{13}C NMR (DMSO-d_6) δ 105.1 (s), 117.1 (d), 118.7 (d), 119.2 (d), 119.4 (d), 121.1 (d), 122.0 (s), 124.7 (s), 124.8 (d), 126.5 (s), 126.9 (s), 127.0 (d), 127.2 (s), 130.3 (s), 147.0 (s). Anal. ($C_{15}H_8Cl_2N_2O$) C, H, N.

General Procedure for the Synthesis of 11-Cyanoisoindolo[2,1-*a*]quinoxalines 5a,c–e. 1-Cyano-2-(2′-aminophenyl)isoindoles **3a,c–e** (3 mmol) were dissolved in formic acid 99% (10 mL) and refluxed until disappearance of the starting material (10−30 h). The reaction mixture was poured into ice water (150 mL), and the resulting precipitate was collected by filtration. The solid was purified by flash chromatography to give the products **5a,c−e**.

11-Cyanoisoindolo[2,1-*a*]quinoxaline 5a. This compound was eluted by using dichloromethane: yield 70%; mp 237−238 °C; IR 2192 (CN) cm^{-1}; ^1H NMR (DMSO-d_6) δ 7.55 (t, 1H, J = 7.2 Hz, H-8), 7.68 (t, 1H, J = 7.2 Hz, H-9), 7.81 (d, 1H, J = 7.2 Hz, H-7), 7.87 (t, 1H, J = 8.0 Hz, H-2), 7.90 (t, 1H, J = 8.0 Hz, H-3), 8.20 (d, 1H, J = 7.2 Hz, H-10), 8.57 (d, 1H, J = 8.0 Hz, H-1), 9.06 (d, 1H, J = 8.0 Hz, H-4), 9.79 (s, 1H, H-6);^{13}C NMR (DMSO-d_6) δ 89.4 (s), 115.4 (s), 115.7 (d), 116.9 (d), 119.8 (s), 120.3 (d), 121.7 (s), 124.7 (d), 127.2 (s), 128.4 (d), 128.5 (d), 129.0 (d), 139.7 (d), 132.2 (s), 138.5 (s), 143.3 (d). Anal. ($C_{16}H_9N_3$) C, H, N.

11-Cyano-3-methoxyisoindolo[2,1-*a*]quinoxaline 5c. This compound was eluted by using dichloromethane: yield 68%; mp 220−221 °C; IR 2193 (CN) cm^{-1}; ^1H NMR (DMSO-d_6) δ 3.97 (s, 3H, CH_3), 7.31 (dd, 1H, J = 9.6, 3.0 Hz, H-2), 7.46 (t, 1H, J = 8.1 Hz, H-8), 7.53 (s, 1H, H-4), 7.58 (t, 1H, J = 8.1 Hz, H-9), 7.90 (d, 1H, J = 8.1 Hz, H-10), 8.19 (d, 1H, J = 8.1 Hz, H-7), 9.06 (d, 1H, J = 9.6 Hz, H-1), 8.81 (s, 1H, H-6);^{13}C NMR (DMSO-d_6) δ 55.8 (q), 90.2 (s), 111.1 (d), 115.6 (s), 117.2 (d), 117.6 (d), 118.6 (d), 118.8 (d), 120.2 (s), 121.2 (s), 122.0 (s), 124.8 (d), 127.9 (d), 132.6 (s), 140.5 (s), 142.3 (d), 159.2 (s). Anal. ($C_{17}H_{11}N_3O$) C, H, N.

11-Cyano-2,3-dimethylisoindolo[2,1-*a*]quinoxaline 5d. This compound was eluted by using dichloromethane:ethyl acetate (98:2): yield 71%; mp 220−221 °C; IR 2193 (CN) cm^{-1}; ^1H NMR (DMSO-d_6) δ 2.45 (s, 3H, CH_3), 2.54 (s, 3H, CH_3), 7.49 (t, 1H, J = 7.5 Hz, H-8), 7.60 (t, 1H, J = 7.5 Hz, H-9), 7.85−7.88 (m, 2H, H-10 and H-4), 8.33 (d, 1H, J = 7.5 Hz, H-7), 8.85 (s, 1H, H-1), 9.44 (s, 1H, H-6);^{13}C NMR (DMSO-d_6) δ 19.2 (q), 20.1 (q), 111.2 (s), 113.1 (s), 115.2 (d), 116.6 (d), 119.0 (d), 119.4 (s), 121.0 (s), 124.0 (d), 124.9 (s), 127.4 (d), 130.0 (d), 132.0 (s), 136.7 (s), 137.3 (s), 138.2 (s), 141.0 (d). Anal. ($C_{18}H_{13}N_3$) C, H, N.

11-Cyano-2,3-dichloroisoindolo[2,1-*a*]quinoxaline 5e. This compound was eluted by using dichloromethane: yield 75%; mp 279−281 °C; IR 2196 (CN) cm^{-1}; ^1H NMR ($CDCl_3$) δ 7.57 (t, 1H, J = 8.3 Hz, H-8), 7.68 (t, 1H, J = 8.3 Hz, H-9), 8.00 (d, 1H, J = 8.3 Hz, H-10), 8.29 (d, 1H, J = 8.3 Hz, H-7), 8.31 (s, 1H, H-1), 9.35 (s, 1H, H-4), 9.46 (s, 1H, H-6);^{13}C NMR ($CDCl_3$) δ 86.9 (s), 96.5 (s), 112.5 (s), 117.6 (d x 2), 119.1 (s), 121.7 (s), 125.8 (s), 128.8 (d x 2), 129.7 (s), 131.8 (d), 143.3 (d x 2), 145.1 (s), 152.3 (s). Anal. ($C_{16}H_7Cl_2N_3$) C, H, N.

Biology. Colchicine and vinblastine were purchased from Sigma-Aldrich (Milan, Italy), Taxol from Cytoskeleton (USA), and Camptothecin from Alexis Biochemicals (Switzerland).

Cell Cultures. Human lymphoblastic leukemia cells (Jurkat) and human lymphoblastoid cells (CEM) were grown in RPMI-1640

medium (Sigma-Aldrich), human intestinal adenocarcinoma (LoVo) were grown in HAM'S F12 medium (Sigma-Aldrich), whereas human nonsmall cell lung carcinoma cells (A-549) and breast adenocarcinoma cells (MCF-7) were grown in DMEM medium (Sigma, USA). All were supplemented with 115 units/mL of penicillin G (Invitrogen, Milan, Italy), 115 μg/mL streptomycin (Invitrogen), and 10% fetal bovine serum (Invitrogen). $LoVo^{Doxo}$ are doxorubicin-resistant subclones of LoVo cells[38] and were grown in complete HAM'S F12 medium supplemented with doxorubicin (0.1 μg/mL). $CEM^{Vbl\text{-}100}$ are a multidrug-resistant line selected against vinblastine.[39] MCF-7 ^{MDR} are human mammary carcinoma exhibiting multidrug resistance and high level of P-gp expression.[40] They were grown in complete DMEM medium supplemented with doxorubicin (0.1 μg/mL).

Cell Cycle Analysis. For flow cytometric analysis of DNA content, 5×10^5 Jurkat cells in exponential growth were treated at different concentrations of the test compound for 24 h. After this incubation period, cells were centrifuged and fixed with ice-cold ethanol (70%), treated with lysis buffer containing RNaseA, and then stained with propidium iodide. Samples were analyzed on a Becton Coulter Epics XL-MCL flow cytometer. For cell cycle analysis, DNA histograms were analyzed by using MultiCycle for Windows (Phoenix Flow Systems, San Diego, CA).

Externalization of Phosphatidylserine. Surface exposure of phosphatidylserine (PS) by apoptotic cells was measured by flow cytometry with a Coulter Cytomics FC500 (Becton Dickinson, USA) by adding Annexin V-FITC to cells according to the manufacturer's instructions (Annexin-V Fluos, Roche Diagnostic, Indianapolis, IN). Simultaneously, the cells were stained with PI. Excitation was set at 488 nm, and the emission filters were at 525 and 585 nm.

Assessment of Mitochondrial Changes. The mitochondrial membrane potential was measured with the lipophilic cation 5,5′,6,6′-tetrachlo-1,1′,3,3′-tetraethylbenzimidazolcarbocyanine (JC-1, Molecular Probes, USA), as described elsewhere.[21] Briefly, after 24 h of treatment, the cells were collected by centrifugation and resuspended in Hank's balanced salt solution (HBSS) containing the JC-1 at a concentration of 1 μM. The cells were then incubated for 10 min at 37 °C, centrifuged, and resuspended in HBSS.

The production of ROS and the oxidation of cardiolipin were measured by flow cytometry by using HE (Molecular Probes, USA) and NAO (Molecular Probes, USA), respectively.[23,24]

After 24 h of treatment, the cells were collected by centrifugation and resuspended in HBSS containing the fluorescence probes HE or NAO at concentrations of 2.5 μM and 100 nM, respectively. The cells were then incubated for 30 min at 37 °C, centrifuged, and resuspended in HBSS. The fluorescence was directly recorded with the flow cytometer by using as excitation wavelength 488 nm and emission at 585 and 530 nm for HE and NAO, respectively.

Mitotic Index Determinations. Exponentially growing Jurkat cells were incubated with test compound for 24 h prior to centrifugation at 400*g* for 5 min and resuspension of the resultant cell pellet in 1 mL of KCl 75 mM at 4 °C. After 20 min, 1 mL of methano−-acetic acid (3:l) as fixative was slowly added under constant mild agitation. Slides were prepared after the cells were repelled, washed twice with 1 mL of fixative, and resuspended in the fixative. After drying, samples were stained with Giemsa solution. A total of 400 cells/treatment was scored for the presence of mitotic figures by optical microscopy, and the mitotic index was calculated as the proportion of cells with mitotic figures.

Immunofluorescence Detection of Microtubule Perturbation. A549 cells were seeded on sterile microscope coverslips. After 24 h, the test compound (5 and 2.5 μM) and vinblastine (1 μM), as reference compound, were added to the culture medium, and cells were then incubated for 18 h. Afterward, cells were fixed with 4% formaldehyde in PBS for 10 min at room temperature, washed three times with PBS, permeabilized in 0.2% Triton X-100 in PBS for 10 min at room temperature, and placed in methanol at −20 °C for 30 min. They were then washed with PBS and incubated for 1 h at 37 °C with 2% bovine serum albumin (BSA) and subsequently, with a mouse monoclonal anti-β-tubulin antibody for 1 h at 37 °C. Slides were washed three times with PBS and incubated with a TRITC-conjugated rat antimouse IgG antibody (diluted 1:200 in 2% BSA) at 37 °C for a further 1 h. Slides were then washed repeatedly with PBS, mounted with mounting medium, and analyzed by confocal microscopy (SP-2, Leica) under green light.

Tubulin Polymerization. The effects of test compounds on the polymerization of microtubule protein isolated from porcine brain were analyzed by using a microtubule polymerization assay kit (Cytoskeleton) following the recommended protocol. Polymerization was followed by fluorescent enhancement because of the incorporation of a fluorescent reporter into microtubules as polymerization occurred. The assay was done in 96-well microtiter plates, and the reaction was initiated by the addition of tubulin. The plate was incubated at 37 °C in a fluorescence microplate reader (Fluoroskan Ascent FL Labsystems), and the fluorescence measurement (λ_{ex} = 355 nm and λ_{em} = 450 nm) was determined every minute for 60 min. As reference compounds, Taxol and colchicine were used.

DNA-Binding Studies. Light absorption spectra were recorded with a Perkin-Elmer Lambda 15 spectrophotometer. Fluorescence spectra were recorded with a Perkin-Elmer LS50B spectrofluorimeter. Measurements were carried out in ETN buffer (10 mM Tris, 1 mM EDTA, and 10 mM NaCl) at 25 °C. To obtain the intrinsic binding constant and the binding-site size as well, absorption spectra of solutions with different [drug]/[DNA] ratios and a constant drug concentration were recorded. The binding isotherms obtained were represented as Scatchard plots[13] and evaluated according to the McGhee and von Hippel model.[12]

Linear Dichroism. LD measurements were performed with a Jasco J500A spectropolarimeter equipped with an IBM PC and a Jasco J interface as reported previously.[41] The sample orientation was produced by a device designed by Wada and Kozawa[42] at a shear gradient of 700 rpm in ETN buffer at pH = 7.0.

Topoisomerase I Assay. Supercoiled pBR322 DNA (Fermentas, Glen Burnie, MD) was incubated with 5 units of human topoisomerase I (Calbiochem, Gibbstown, NJ) at 37 °C for 30 min in relaxation buffer (50 mM Tris-HCl pH = 7.8, 50 mM KCl, 10 mM $MgCl_2$, 1 mM dithiothreitol, and 1 mM EDTA) in the presence of various concentrations of the drug. Reactions were terminated by adding 1% SDS and an additional digestion with 50 μg/mL proteinase K at 37 °C for 30 min. DNA samples were then added to loading buffer and electrophoresed in a 1% agarose gel at room temperature overnight at 20 V. After staining in ethidium bromide solution, the gel was washed with water, and the DNA bands were detected under UV radiation with a UV transilluminator. Photographs were taken with a digital photocamera Kodak DC256, and the quantization of the bands was achieved by image analyzer software Quantity One (BIO RAD, Milan, Italy). Similar experiments were performed by using ethidium-containing agarose gels.

Topoisomerase II Assay. Assay mixtures were prepared by using 125 ng of supercoiled pBR322 plasmid, 2 units of human topoisomerase IIα (Sigma), and 0−50 μM of selected compounds in aqueous solution (50 mM Tris-HCl pH = 8.0, 10 mM $MgCl_2$, 120 mM KCl, 0.5 mM DTT, and 30 μg of BSA). Reactions were carried out and then stopped after an incubation period of 30 min. Gel electrophoresis was performed as described above for topoisomerase I.

Caspase Assay. Jurkat cells were treated in the presence of the test compounds, and after 24 h, the cells were harvested, washed, and resuspended in HBSS buffer containing the cell-permeable substrates for caspase-3 (FITC-DEVD-fmk, Bender Medsystem, Burlingame, CA), caspase-8 (FITC-IETD-fmk, Bender Medsystem), and caspase-9 (FITC-LEDH-fmk, Bender Medsystem). After 1 h of incubation at 37 °C, the cells were washed and analyzed by flow cytometry by using the FL-1 channel.

Acknowledgment. This work was financially supported by Ministero dell'Istruzione dell'Università e della Ricerca. We thank the National Cancer Institute (Bethesda, MD) and especially Dr. V. L. Narayanan and his team for the antitumor tests reported in this paper. G.V. thanks Fondazione Città della Speranza for its financial support.

Supporting Information Available: Results from elemental analysis. This material is available free of charge via the Internet at http://pubs.acs.org.

References

(1) Sengupta, S. K. Inhibitors of DNA topoisomerases. In *Cancer Chemotherapeutic Agents*; Foye W. O., Ed.; American Chemical Society: DC, 1995; pp 205–217.

(2) (a) Grimm, C.; Ehrenberger, K.; Thurnher, D. Preparation containing 1-diethylaminoethyl-3-quinoxalin-2-one derivatives for treatment cancer. WO 2005105098; CAN 143:452851, 2005. (b) Alleca, S.; Corona, P.; Loriga, M.; Paglietti, G.; Loddo, R.; Mascia, V.; Busonera, B.; La Colla, P. Quinoxaline chemistry. Part 16. 4-Substituted aniline and 4-substituted phenoxymethyl pyrrolo[1,2-a]quinoxalines and N-[4-(pyrrolo[1,2-a]quinoxalin-4-yl)amino and hydroxymethyl]benzoyl glutamates. Synthesis and evaluation of in vitro biological activity. *Il Farmaco* **2003**, *58*, 639–650. (c) Miyata, F.; Yoshida, S.; Yamori, T.; Katoh, T. An efficient expeditious synthesis of novel 5H-naphth[1′,2′:5,6][1,4]oxazino[2,3-b]quinoxalin-5-one and its unique inhibitory activity against a panel of human cancer cell lines. *Heterocycles* **2001**, *54*, 619–622.

(3) Lawrence, D. S.; Copper, J. E.; Smith, C. D. Structure-activity studies of substituted quinoxalinones as multiple-drug-resistance antagonists. *J. Med. Chem.* **2001**, *44*, 594–601.

(4) Nguyen, C. H.; Fan, E.; Riou, J.; Bissery, M. C.; Vrignaud, P.; Lavelle, F.; Bisagni, E. Synthesis and biological evaluation of amino-substituted benzo[f]pyrido[4,3-b] and pyrido[3,4-b]quinoxalines: A new class of antineoplastic agents. *Anti-Cancer Drug Des.* **1995**, *10*, 277–297.

(5) Abadi, A. H. 5-Substituted 2-bromoindolo[3,2-b]quinoxalines. A class of potential antitumor agents with cdc25 phosphatase inhibitory properties. *Arch. Pharm. Med. Chem.* **1998**, *331*, 352–358.

(6) See for example (a) Diana, P.; Barraja, P.; Lauria, A.; Montalbano, A.; Almerico, A. M.; Dattolo, G.; Cirrincione, G. Pyrrolo[2,1-d]-[1,2,3,5]tetrazine-4(3H)-ones, a new class of azolotetrazines with potent antitumor activity. *Bioorg. Med. Chem.* **2003**, *11*, 2371–2380. (b) Cirrincione, G.; Almerico, A. M.; Barraja, P.; Diana, P.; Lauria, A.; Passannanti, A.; Musiu, C.; Pani, A.; Murtas, P.; Minnei, C.; Marongiu, M. E.; La Colla, P. Derivatives of the new ring system indolo[1,2-c]benzo[1,2,3]triazine with potent antitumor and antimicrobial activity. *J. Med. Chem.* **1999**, *42*, 2561–2568. (c) Barraja, P.; Diana, P.; Lauria, A.; Passannanti, A.; Almerico, A. M.; Minnei, C.; Longu, S.; Congiu, D.; Musiu, C.; La Colla, P. Indolo[3,2-c]cinnolines with antiproliferative, antifungal, and antibacterial activity. *Bioorg. Med. Chem.* **1999**, *7*, 1591–1596.

(7) Dyker, G.; Stirner, W.; Henkel, G. Oxidative heterocyclization of 2-alkylylbenzaldehydes with 1,2-phenylendiamine. *Eur. J. Org. Chem.* **2000**, 1433–1441.

(8) Paolini, J. P.; Palopoli, F. P.; Lendvay, L. J.; Huffman, J. Pyrido[2′,1′:2,3]imidazo[4,5-c]isoquinoline and the alkylation of pyrido[2′,1′:2,3]imidazo[4,5-c]isoquinolin-5(6H)-one. *J. Heterocycl. Chem.* **1987**, *24*, 549–553.

(9) Monks, A.; Scudiero, D.; Skehaan, P.; Shoemaker, R.; Paull, K.; Vitisca, D.; Hose, C.; Langley, J.; Cronise, P.; Vaigro-Wolff, A.; Gray-Goodrich, M.; Campbell, H.; Mayo, J.; Boyd, M. R. Feasibility of a high-flux anticancer drug screen using a diverse panel of cultured human tumor cell lines. *J. Natl. Cancer Inst.* **1991**, *83*, 757–766.

(10) Boyd, M. R.; Paull, K. D. Some practical considerations and applications of the national cancer institute in vitro anticancer drug discovery screen. *Drug Dev. Res.* **1995**, *34*, 91–109.

(11) Bonne, D.; Heusele, C.; Simon, C.; Pantaloni, D. 4′,6-Diamidino-2-phenylindole, a fluorescent probe for tubulin and microtubule. *J. Biol. Chem.* **1985**, *260*, 2819–2825.

(12) McGhee, D.; von Hippel, P. H. Theorical aspects of DNA-protein interactions: Co-operative and non-co-operative binding of large ligands to a one-dimensional homogeneus lattice. *J. Mol. Biol.* **1974**, *6*, 469–489.

(13) Schatchard, G. The attraction of proteins for small molecules and ions. *Ann. N.Y. Acad. Sci.* **1949**, *51*, 660–672.

(14) Lyng, R.; Härd, T.; Nordén, B. Induced circular dichroism of DNA intercalators: Electric dipole allowed transitions. *Biopolymers* **1987**, *26*, 1327–1345.

(15) Lyng, R.; Rodger, A.; Nordén, B. The circular dichroism of ligand-DNA systems. I. Poly(dG-dC) B-DNA. *Biopolymers* **1992**, *31*, 1709–1720.

(16) Lyng, R.; Rodger, A.; Nordén, B. The circular dichroism of ligand-DNA systems. II. Poly(dA-dT) B-DNA. *Biopolymers* **1992**, *32*, 1201–1214.

(17) Norden, B. Linear dichroism spectroscopy. *Appl. Spectrosc. Rev.* **1978**, *14*, 157–248.

(18) Nordén, B.; Kubista, M.; Kurucsev, T. Linear dichroism spectroscopy of nucleic acid. *Q. Rev. Biophys.* **1992**, *25*, 51–171.

(19) Vermes, I.; Haanen, C.; Steffens-Nakken, H.; Reutelingsperger, C. A novel assay for apoptosis. Flow cytometric detection of phosphatidylserine expression on early apoptotic cells using fluorescein labelled Annexin V. *J. Immunol. Methods* **1995**, *184*, 39–51.

(20) Bernardi, P.; Scorrano, L.; Colonna, R.; Petronilli, V.; Di Lisa, F. Mitochondria and cell death. Mechanistic aspects and methodological issues. *Eur. J. Biochem.* **1999**, *264*, 678–701.

(21) Green, D. R.; Kroemer, G. The pathophysiology of mitochondrial cell death. *Science* **2005**, *305*, 626–629.

(22) Salvioli, S.; Ardizzoni, A.; Franceschi, C.; Cossarizza, A. JC-1 but not DiOC6(3) or rhodamine 123 is a reliable fluorescent probe to asses φ changes in intact cells: Implications for studies on mitochondrial functionality during apoptosis. *FEBS Lett.* **1997**, *411*, 77–82.

(23) Zamzami, N.; Marchetti, P.; Castedo, M.; Decaudin, D.; Macho, A.; Hirsch, T.; Susin, S. A.; Petit, P. X.; Mignotte, B.; Kroemer, G. Sequential reduction of mitochondrial transmembrane potential and generation of reactive oxygen species in early programmed cell death. *J. Exp. Med.* **1995**, *182*, 367–377.

(24) Rothe, G.; Valet, G. Flow cytometric analysis of respiratory burst activity in phagocytes with hidroethidine and 2′,7′-dichlorofluorescein. *J. Leukocyte Biol.* **1990**, *47*, 440–448.

(25) Petit, J. M.; Maftah, A.; Ratinaud, M. H.; Julien, R. 10-N-nonyl acridine orange interacts with cardiolipin and allows the quantification of this phospholipid in isolated mitochondria. *Eur. J. Biochem.* **1992**, *209*, 267–273.

(26) Gallet, P. F.; Maftah, A.; Petit, J. M.; Denis-Gay, M.; Julien, R. Direct cardiolipin assay in yeast using the red fluorescence emission of 10-N-nonyl acridine orange. *Eur. J. Biochem.* **1995**, *228*, 113–119.

(27) Thomberry, A. N.; Lazebnik, Y. Caspases: Enemies within. *Science* **1998**, *281*, 1312–1316.

(28) Earshaw, W. C.; Martins, L. M.; Kaufmann, S. H. Mammalian caspases: Structure, activation, substrates and functions during apoptosis. *Annu. Rev. Biochem.* **1999**, *68*, 383–424.

(29) Hengartner, G. The biochemistry of apoptosis. *Nature* **2000**, *407*, 770–776.

(30) Susin, S. A.; Lorenzo, H. K.; Zamzami, N.; Marzo, I.; Brenner, C.; Larochette, N.; Prevost, M. C.; Alzari, P. M.; Kroemer, G. Mitochondrial release of caspase-2 and -9 during apoptotic process. *J. Exp. Med.* **1999**, *189*, 381–393.

(31) Susin, S. A.; Zamzami, N.; Castedo, M.; Dugas, E.; Wang, H. G.; Geley, S.; Fassy, F.; Reed, J. C.; Kroemer, G. The central executioner of apoptosis. Multiple link between protease activation and mitochondria in Fas/apo-1/Cd95- and ceramide-induced apoptosis. *J. Exp. Med.* **1997**, *186*, 25–37.

(32) Pourquier, P.; Pommier, Y. Topoisomerase I-mediated DNA damage. *Adv. Cancer Res.* **2000**, *80*, 189–216.

(33) Ihmels, H.; Otto, D. Intercalation of organic dye molecules into double-stranded DNA: General principles and recent developments. *Top. Curr. Chem.* **2005**, *258*, 161–204.

(34) Masuda, A.; Maeno, K.; Nacagawa, T.; Saito, H.; Takahashi, T. Association between mitotic spindle checkpoint impairment and susceptibility to the induction of apoptosis by anti-microtubule agents in human lung cancers. *Am. J. Pathol.* **2003**, *163*, 1109–1116.

(35) Mollinedo, F.; Gajate, C. Microtubules, microtubule-interfering agents and apoptosis. *Apoptosis* **2003**, *8*, 413–450.

(36) Kluza, J.; Lansiaux, A.; Vattez, N.; Matthieu, C.; Osheroff, N.; Bailly, C. Apoptotic response of HL-60 human leukemia cells to the antitumor drug TAS-103. *Cancer Res.* **2000**, *60*, 4077–4084.

(37) Kluza, J.; Gallego, M. A.; Loyens, A.; Beauvillain, J. C.; Sousa-Faro, J. M.; Cuevas, C.; Marchetti, P.; Bailly, C. Cancer cell mitochondria are direct proapoptotic targets for the marine antitumor drug lamellarin D. *Cancer Res.* **2006**, *66*, 3177–3187.

(38) Toffoli, G.; Viel, A.; Tuimoto, I.; Bisconti, G.; Rossi, G.; Baoiocchi, M. Pleiotropic-resistant phenotype is a multifactorial phenomenon in human colon carcinoma cell lines. *Br. J. Cancer* **1991**, *63*, 51–56.

(39) Dupuis, M.; Flego, M.; Molinari, A.; Cianfriglia, M. Saquinavir induces stable and functional expression of the multidrug transporter P-glycoprotein in human CD4 T-lymphoblastoid CEMrev cells. *HIV Med.* **2003**, *4*, 338–345.

(40) Gudas, J. M.; Nguyen, H.; Li, T.; Sadzewicz, L.; Robey, R.; Wosikowsky, K.; Cowan, K. Drug-resistant breast cancer cells frequently retain expression of a functional wild-type p53 protein. *Carcinogenesis* **1996**, *17*, 1417–1427.

(41) Viola, G.; Dall'Acqua, F.; Gabellini, N.; Moro, S.; Vedaldi, D.; Ihmels, H. Indolo[2,3-b]-quinolizinium bromide: An efficient intercalator with DNA-photodamaging properties. *ChemBioChem* **2002**, *3*, 101–109.

(42) Wada, A.; Kozawa, S. Instrument for the studies of differential flow dichroism of polymer solutions. *J. Polym. Sci., Part A* **1964**, *2*, 853–864.

JM070834T